



# The Determination of ClNO<sub>2</sub> via Thermal Dissociation-Tunable Infrared Laser Direct Absorption Spectroscopy

John W. Halfacre<sup>1</sup>, Lewis Marden<sup>1</sup>, Marvin D Shaw<sup>1</sup>, Lucy J Carpenter<sup>1</sup>, Emily Matthews<sup>2</sup>, Thomas J. Bannan<sup>2</sup>, Hugh Coe<sup>2,3</sup>, Scott C. Herndon<sup>4</sup>, Joseph R. Roscioli<sup>4</sup>, Christoph Dyroff<sup>4</sup>, Tara I. Yacovitch<sup>4</sup>, Patrick R. Veres<sup>5\*</sup>, Michael Robinson<sup>5,6</sup>, Steven S. Brown<sup>5,7</sup>, Pete M. Edwards<sup>1,8</sup>

<sup>1</sup>Wolfson Atmospheric Chemistry Laboratories, Department of Chemistry, University of York, Heslington, York, YO10 5DD, UK

<sup>2</sup>Department of Earth and Environmental Science, Centre for Atmospheric Science, School of Natural Sciences, The University of Manchester, Manchester M13 9PL, UK

<sup>3</sup>National Centre for Atmospheric Science, University of Manchester, Manchester, UK

<sup>4</sup>Aerodyne Research, Inc., Billerica, MA, 01821, USA

<sup>5</sup>Chemical Sciences Laboratory, National Oceanic and Atmospheric Administration, Boulder, CO, 80305, USA

<sup>6</sup>Cooperative Institute for Research in Environmental Sciences, University of Colorado, Boulder, CO, 80305, USA

<sup>7</sup>Department of Chemistry, University of Colorado, Boulder, CO 80309, USA

<sup>8</sup>National Centre for Atmospheric Science, University of York, York, UK

\*Now at National Science Foundation, National Center for Atmospheric Research, Boulder, CO, 80301, USA

Correspondence to: John Halfacre ([john.halfacre@york.ac.uk](mailto:john.halfacre@york.ac.uk)), Pete Edwards ([pete.edwards@york.ac.uk](mailto:pete.edwards@york.ac.uk))

**Abstract.** Nitryl chloride (ClNO<sub>2</sub>) is a reservoir species of chlorine atoms and nitrogen oxides, both of which play important roles in atmospheric chemistry. To date, all ambient ClNO<sub>2</sub> observations have been obtained by chemical ionization mass spectrometry (CIMS). In this work, Thermal Dissociation Tunable Infrared Laser Differential Absorption Spectrometer (TD-TILDAS) is shown to be a viable method for quantifying ClNO<sub>2</sub> in laboratory and field settings. This technique relies on the thermal dissociation of ClNO<sub>2</sub> to create chlorine radicals, which undergo fast reactions with hydrocarbons to produce hydrogen chloride (HCl) that is detectable by the TILDAS instrument. Complete quantitative conversion of ClNO<sub>2</sub> to HCl was achieved at temperatures > 400°C, achieving 1 Hz measurement precision of  $11 \pm 1$  pptv ( $3\sigma$  limits of detection of  $34 \pm 2$  pptv) during laboratory comparisons with other ClNO<sub>2</sub> detection methods. After blank- and line loss-corrections, method accuracy is estimated to be within  $\pm 5\%$ . Performance metrics of TD-TILDAS during ambient sampling were a 1 Hz precision of  $19 \pm 1$  pptv and  $3\sigma$  limits of detection of  $57 \pm 3$  pptv, which is directly comparable to previously reported ClNO<sub>2</sub> detection by quadrupole CIMS. Thus, TD-TILDAS can provide an alternative analytical approach for a direct measurement of ClNO<sub>2</sub> that can complement existing datasets and future studies. The quantitative nature of TD-TILDAS also makes it a potentially useful tool for the calibration of CIMS instruments. However, interpretation of ambient data may be potentially complicated by interference from unaccounted-for sources of thermolabile chlorine.

## 1 Introduction

Nitryl chloride (ClNO<sub>2</sub>) is an important nighttime reservoir of two highly reactive atmospheric species: atomic Cl and NO<sub>2</sub>. Atomic Cl radicals play multifaceted roles in oxidation chemistry throughout the boundary layer (Simpson et al., 2015),



including hydrocarbon oxidation (Atkinson et al., 2006a, and references therein), ozone production and destruction (Halfacre and Simpson, 2022; Liao et al., 2014; Sarwar et al., 2012, 2014; Simon et al., 2009; Wang et al., 2016), and mercury depletion (Driscoll et al., 2013). However, the quantitative magnitude to which they affect these processes remains an open question. On the other hand, NO<sub>2</sub> is one of the principal components of photochemical smog and the major anthropogenic precursor for ozone production. Accounting for all sources of NO<sub>2</sub> is therefore important for accurately informing chemical and air quality models.

The first in situ observation of ambient ClNO<sub>2</sub> was reported by Osthoff et al. (2008) utilising chemical ionization mass spectrometry (CIMS) in the polluted marine boundary layer. CIMS has since been used in a multitude of studies for additional ClNO<sub>2</sub> observations worldwide, including North America (Jaeglé et al., 2018; Lee et al., 2018a, b; Mielke et al., 2011; Riedel et al., 2012, 2013; Thornton et al., 2010; Wagner et al., 2013; Young et al., 2012), Europe (Bannan et al., 2015; Phillips et al., 2012; Sommariva et al., 2018; Tan et al., 2022), Asia (Le Breton et al., 2018; Liu et al., 2017; Tham et al., 2016, 2018; Wang et al., 2022, 2016, 2017; Xia et al., 2020; Ye et al., 2021; Yu et al., 2020; Zhou et al., 2018), in the presence of snow/ice (Kercher et al., 2009; McNamara et al., 2020), and in indoor air quality studies (Moravek et al., 2022). Limits of detection are often reported at 10<sup>0</sup> pptv under 25–30 s averaging times, (Bannan et al., 2015; Kercher et al., 2009; McNamara et al., 2020; Mielke et al., 2011), and has been recently reported at sub-pptv for 1 s measurements (Decker et al., 2024). Typical observed mixing ratios range from 10<sup>1</sup> – 10<sup>3</sup> pptv, with the highest levels observed in coastal polluted regions, where sources of nitrogen oxides and Cl-rich aerosols are plentiful (Wang et al., 2019, 2021, and references therein).

While CIMS is a highly effective technique, ClNO<sub>2</sub> quantitation involves non-trivial calibration work. A laboratory source of ClNO<sub>2</sub> may be readily generated by flowing a known amount of N<sub>2</sub>O<sub>5</sub> across a Cl<sup>-</sup>-containing salt bed (or Cl<sub>2</sub> across NO<sub>2</sub><sup>-</sup>-containing salt bed), but its quantitation assumes unit conversion out of the salt bed (e.g., Osthoff et al., 2008) or requires additional equipment to observe ClNO<sub>2</sub> thermal dissociation products, such as a N<sub>2</sub>O<sub>5</sub>-cavity ring down spectrometer (CRDS) (Thaler et al., 2011) or a cavity attenuated phase shift spectrometer (CAPS) (e.g., Tan et al., 2022). Further, I<sup>-</sup>-based CIMS demonstrates variable sensitivities based on the temperature and relative humidity of the ion-molecule reactor, thereby requiring substantial laboratory work to develop humidity- and temperature-dependent calibration factors (Lee et al., 2014; Robinson et al., 2022). Thus, there is an opportunity to innovate a method that can detect ClNO<sub>2</sub> directly without the need for supplemental instrumentation.

The advantages of optical methods include analyte specificity and near absolute detection, utilizing well-defined physical absorption properties, and requiring only infrequent calibrations or method validation procedures. Thaler et al. (2011) previously used a CRDS system (tuned for the detection of peroxyacyl nitrates) to detect ClNO<sub>2</sub> under laboratory conditions, achieving CIMS-competitive metrics (e.g., reported 20 pptv limit of detection for 1 minute averaging). This was achieved by flowing sample air through both an unheated reference pathway and a heated (450 °C) sample pathway, under which ClNO<sub>2</sub> would thermally dissociate into Cl radicals and NO<sub>2</sub> (Reaction R1).



The difference in observed NO<sub>2</sub> signal between the two channels provided a quantitative ClNO<sub>2</sub> measurement. However, its use for conducting field measurements was reported to be limited, as the thermal degradation of alkyl nitrates (i.e., PAN) into NO<sub>2</sub> cannot be distinguished from NO<sub>2</sub> originating from ClNO<sub>2</sub> due to overlapping thermal dissociation profiles.

For this same thermal-dissociation setup, product chlorine radicals will react quickly (e.g., Cl radical lifetime of 0.2 s for typical CH<sub>4</sub> mixing ratios of 2 ppmv and  $k_{298} = 1 \times 10^{-13} \text{ cm}^3 \text{ molecule}^{-1} \text{ s}^{-1}$  (Bryukov et al., 2002)) with ambient



hydrocarbons (e.g., methane) to form hydrogen chloride (HCl), which is a stable reservoir species for reactive chlorine (Reaction R2).



Several optical methods for the high-frequency and precise detection of HCl have recently been reported that overcome historical challenges with its sampling (Furlani et al., 2021; Hagen et al., 2014; Halfacre et al., 2023; Wilkerson et al., 2021), making them attractive candidates for an alternative thermal dissociation approach for the detection of ClNO<sub>2</sub>. In this work, we demonstrate the coupling of a thermal dissociation furnace to HCl-TILDAS (TD-TILDAS) for quantitative detection of ClNO<sub>2</sub> as HCl. Compared with CIMS, TD-TILDAS is a lower cost method for determining ClNO<sub>2</sub> mixing ratios, involving less experimental calibration work and simpler data processing as a direct method.

## 2 Methods

### 2.1 ClNO<sub>2</sub> Generation

ClNO<sub>2</sub> was synthesized by flowing Cl<sub>2</sub> across a nitrite-rich slurry, as described by Thaler et al. (2011) and shown by Reaction R3.



However, it is believed the ClNO<sub>2</sub>, once produced, may react further by dissolving into the water, hydrolyzing, and producing nitronium and chloride ions (R4) (Frenzel et al., 1998).



The nitronium ion can then react with NO<sub>2</sub><sup>-</sup> to produce N<sub>2</sub>O<sub>4</sub>, which exists in equilibrium with NO<sub>2</sub> (R5).



As detailed by Thaler et al. (2011), this chemistry can be mitigated by minimizing the residence time of ClNO<sub>2</sub> in the reaction vessel and, to a lesser extent, by increasing the Cl<sup>-</sup> content of the slurry to encourage the equilibrium in R4 towards ClNO<sub>2</sub>. Therefore, we composed our slurry using sodium chloride (>99.5% pure, BioXtra, Sigma Aldrich product no S7653-5KG, USA) and sodium nitrite (99%, extra pure, Acros Organics Code 196620010, Belgium) at a mole ratio of 100:1 Cl<sup>-</sup>:NO<sub>2</sub><sup>-</sup>, wetting with 18MΩ deionized water (Millipore). The slurry was housed in ~10 cm of 1.25 cm diameter PFA tubing. Varied flow rates (0.5-5 mL min<sup>-1</sup>) of 10 ppmv Cl<sub>2</sub> (diluted in nitrogen, BOC product no. 150916-AV-B, United Kingdom) were injected into a dilution flow (ranging from 200-2499.5 mL min<sup>-1</sup>) of NO<sub>x</sub>-scrubbed compressed air (using trap composed of 50% Sofnofil (Molecular Products Ltd., Essex, United Kingdom) and 50% activated carbon) that was subsequently passed over the slurry, generating ClNO<sub>2</sub>. A portion of the dilution flow was directed into a bubbler containing 18MΩ deionized water prior to entering the slurry to maintain a humid environment and prevent the slurry from drying out. A schematic diagram of this setup is presented in Fig. 1a.



## 116 2.2 TD-TILDAS

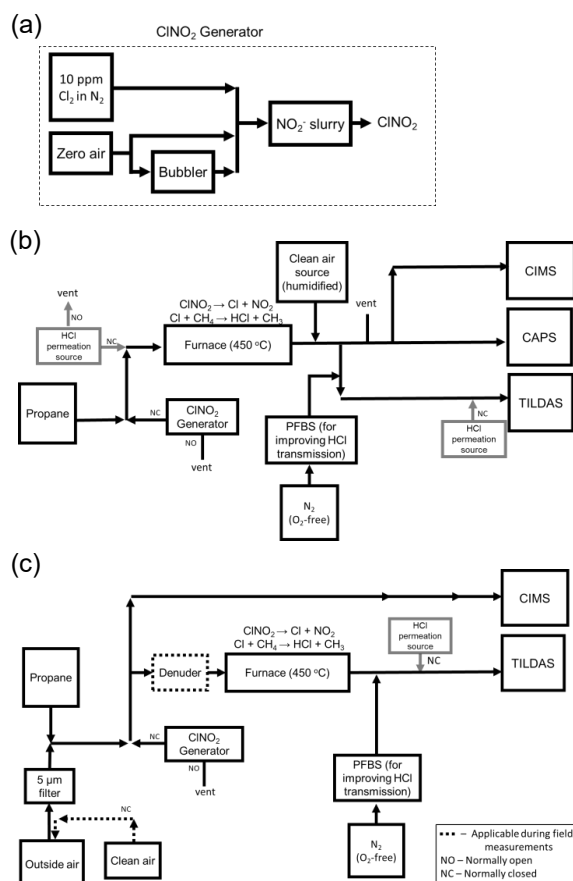
117 The TILDAS instrument and operation technique have been well-described previously (McManus et al., 2011, 2015). HCl-  
 118 TILDAS was developed by Aerodyne Research, Inc. and characterized by Halfacre et al. (2023). Briefly, air is sampled at 3.0  
 119 L min<sup>-1</sup> through a heated (50 °C) quartz “inertial inlet,” which is a type of virtual impactor used to remove particles >300 nm  
 120 from the sample matrix. Sample air continues its flow through 3 m of heated (50 °C) tubing into the Herriott cell (204 m  
 121 pathlength) inside the TILDAS. HCl is then detected via a mid-IR inter-band cascade laser that probes the strong R(1) H<sup>35</sup>Cl  
 122 absorption line at 2925.89645 cm<sup>-1</sup> within the (1-0) rovibrational absorption band (Guelachvili et al., 1981).

123 Nitryl chloride was converted to HCl for detection by TILDAS via thermal dissociation and the subsequent reaction of Cl  
 124 radicals with hydrocarbons, namely methane (Reactions R1-R2) (Thaler et al., 2011). The sample flow was additionally spiked  
 125 with propane (BOC Limited, product no. 34-A) to a mixing ratio of 5 ppmv to ensure reaction completeness and outcompete  
 126 Cl wall losses. Next, the sample was directed to a 90 cm length of quartz tubing (9.5 mm OD, 7.5 mm ID) housed within a  
 127 furnace (Carbolite Gero TS1 12/60/450) upstream of the inertial inlet. Sixty centimetres of this tubing is held within the heated  
 128 region of the furnace, resulting in a residence time of ~500 ms under a flow rate of 3 L min<sup>-1</sup>. To mitigate HCl surface  
 129 interactions after ClNO<sub>2</sub>-conversion, perfluorobutane-1-sulfonic acid (PFBS; Merck, product no. 562629, United Kingdom)  
 130 vapor was introduced just after the furnace to improve HCl transmission to the TILDAS inlet (Halfacre et al., 2023; Roscioli  
 131 et al., 2016). As detailed by Halfacre et al. (2023), a flow (50-75 mL min<sup>-1</sup>) of oxygen-free nitrogen was flowed into the  
 132 headspace of a Teflon bubbler containing 5 g of PFBS, thereby flushing the PFBS vapor into the sample line. A schematic  
 133 diagram of this setup is presented in Fig. 1b.

134 The major sources of uncertainty with using TD-TILDAS to detect ClNO<sub>2</sub> include the degree of ClNO<sub>2</sub> conversion  
 135 to HCl, instrument noise, background drifts, and potential line losses of HCl. Confirmation of the unit conversion of ClNO<sub>2</sub> to  
 136 HCl was confirmed by modelling and laboratory experiments (see Sects. 3.1 and 3.2). Instrument noise and background drifts  
 137 were assessed regularly from blanks. For laboratory experiments, blanks were performed by sampling the ClNO<sub>2</sub> standard  
 138 (Sect. 2.1) diluted in NO<sub>x</sub>-scrubbed compressed air through the unheated furnace. This dilution air was generated using an air  
 139 compressor and dehumidifying system (dew point approximately -60 °C, absolute water vapor concentration ~ 0.01%). To  
 140 vary sample humidity, carrier gas flow was split such that varied amounts were passed through a bubbler containing deionized  
 141 water. Concerning line losses of HCl, the only source of HCl will be from ClNO<sub>2</sub> conversion during laboratory experiments,  
 142 and therefore line losses were assessed between the furnace and the inertial inlet. As detailed in Fig. 1b, 30 mL min<sup>-1</sup> of flow  
 143 from a homemade HCl permeation source (Furlani et al., 2021; Halfacre et al., 2023) was injected alternatingly before the  
 144 furnace and just before the inertial inlet to determine loss of HCl over this region. So long as unit conversion of ClNO<sub>2</sub> to HCl  
 145 can be confirmed and blank / line losses are corrected, this method will be as accurate as the TILDAS is for detecting HCl,  
 146 which was previously found to be within the 5% tolerance of a commercial HCl cylinder with a certified concentration  
 147 (Halfacre et al., 2023).

148 For ambient sampling (Fig. 1c), an additional 5m of 1.25 cm OD PTFE Teflon was added before the tee that splits  
 149 the CIMS and TILDAS flow paths to sample outside air. A 5 µm PFA Teflon filter was also installed to collect particulates,  
 150 reducing the potential for HCl displacement through thermodynamic partitioning of particulate Cl that would otherwise enter  
 151 the heated furnace (Huffman et al., 2009). Blank air was generated by pumping ambient air through a 50% activated carbon /  
 152 50% Sofnofil scrubber, which was found to effectively remove ClNO<sub>2</sub> from the sample stream. The pump (KNF model  
 153 N035.1.2AN.18) was able to overblow the sample inlet at a flow rate of ~25 L min<sup>-1</sup>. This approach is favoured over the use  
 154 of synthetic cylinder air as significant changes in sample humidity can result in release of HCl from surfaces (Halfacre et al.,  
 155 2023). Blanks were performed for 10 minutes every 30 minutes to ensure the instrument had enough time to respond and adjust

156 to a stable background value. Additionally, ambient measurements will include HCl, which would act as an interference for  
 157 ClNO<sub>2</sub> observations. To obviate this, a denuder (coating of 2% Na<sub>2</sub>CO<sub>3</sub> and 2% glycerol dissolved in 50% water and 50%  
 158 methanol) was installed before the furnace to selectively remove acidic gases (e.g., HCl, HNO<sub>3</sub>) that may influence  
 159 quantitation. While effective for this purpose, the denuder was also found to affect ClNO<sub>2</sub> throughput, with a freshly coated  
 160 denuder causing as much as 55% loss of the ClNO<sub>2</sub> standard mixing ratio. As such, the ClNO<sub>2</sub> standard (Sect. 2.1) was sampled  
 161 in dry air before and after overnight experiments to estimate how this loss process evolved over the course of an experiment.  
 162 In contrast to the laboratory experiment configuration, permeation source HCl in blank air was only injected just downstream  
 163 of the furnace mid-experiment. Losses were assessed by comparing this observed HCl injection value to pre- and post-  
 164 experiment injections over dry compressed air. Injections of HCl and ClNO<sub>2</sub> standards was controlled using 3-way Teflon  
 165 solenoid valves (MasterFlex Model no. 01540-18, Cole Parmer, United Kingdom).



166  
 167 **Figure 1** Experimental schematic diagrams for (a) generating ClNO<sub>2</sub>, b) laboratory comparison measurements between CIMS,  
 168 TILDAS, and CAPS NO<sub>2</sub>, and (b) calibration/field sampling between CIMS and TILDAS. Note that “NO” stands for “normally  
 169 open” and “NC” stands for “normally closed” in reference to solenoid valves that control the flow direction for these items.

### 170 2.3 Supporting Instrumentation

171 To confirm the efficacy of TD-TILDAS as a valid quantitative method for ClNO<sub>2</sub> detection, testing was performed  
 172 simultaneously with a Cavity Attenuated Phase Shift (CAPS) NO<sub>2</sub> instrument (Sect. 2.3.1) and Time of Flight-Chemical  
 173 Ionization Mass Spectrometer (Sect. 2.3.2), both of which have previously reported as ClNO<sub>2</sub> detection methods.



### 174 2.3.1 Cavity Attenuated Phase Shift (CAPS) NO<sub>2</sub>

175 ClNO<sub>2</sub> mixing ratios observed by the TILDAS were confirmed via simultaneous detection of the NO<sub>2</sub> product of ClNO<sub>2</sub> thermal  
 176 dissociation using a commercial Cavity Attenuated Phase Shift NO<sub>x</sub> detector (Teledyne T500U CAPS). Briefly, emission from  
 177 a LED (emission centred around 425 nm) is reflected across two spherical mirrors and absorbed by NO<sub>2</sub> in the optical cell.  
 178 This difference in light is detected by a photodiode and quantified based on its absorbance via the Beer-Lambert Law. The  
 179 instrument was calibrated using gas-phase titration of NO by O<sub>3</sub> to produce varied concentrations of NO<sub>2</sub>. A 1ppm NO in  
 180 nitrogen cylinder (certified 982 ppb, NPL) was used to verify the concentration of NO in a 25ppm NO in nitrogen working  
 181 standard (BOC). A multigas blender (EnviroNics S6100) was used to generate a range of O<sub>3</sub> concentrations (range 0-130 ppbv)  
 182 for titrating some of the NO (NO in excess, 200 ppbv) into NO<sub>2</sub>, and the decrease in the NO concentrations was measured  
 183 using a calibrated NO<sub>x</sub> instrument (Teledyne API Chemiluminescence T200). The NO<sub>2</sub> introduced to the CAPS instrument is  
 184 thus the sum of the drop of NO from the added ozone and the NO<sub>2</sub> already present in the working standard. The T200 NO<sub>x</sub>  
 185 instrument was also used to measure ambient air alongside the CAPS (range 0-25 ppbv), and these data are presented in Fig.  
 186 A1.

### 187 2.3.2 Time of Flight Chemical Ionisation Mass Spectrometry (CIMS)

188 ClNO<sub>2</sub> was additionally detected using a VOCUS high-resolution chemical ionization time-of-flight CIMS (Tofwerk,  
 189 Switzerland) with a VOCUS AIM reactor and using iodide (I<sup>-</sup>) as a reagent ion gas. A complete description of this instrument  
 190 and its operational principles are described in detail by Riva et al. (2024). Briefly, sample gas is drawn into the sampling inlet  
 191 and pulled through a critical orifice (0.475 mm) and PFA Teflon sample flow guide into a conical ion-molecule reactor (IMR)  
 192 at a flow rate of 1.8 L min<sup>-1</sup>. The IMR was held at a constant pressure of 50 mbar using a vacuum pump (IDP3, Agilent  
 193 Technologies) and temperature controlled to 50 °C. The reagent ion source was a permeation tube containing trace amounts of  
 194 CH<sub>3</sub>I dissolved in benzene (Tofwerk). Ultra-high purity, oxygen-free N<sub>2</sub> gas (generated by flowing compressed air through  
 195 gas with a commercial N<sub>2</sub> generator, Infinity NM32L, Peak Scientific Instruments, UK) is continually flowed over the  
 196 permeation tube to flush the gaseous CH<sub>3</sub>I/benzene mixture into a compact vacuum ultraviolet ion source (VUV). Within the  
 197 VUV, UV light emitted from a Kr lamp (116.486 nm and 123.582 nm) is absorbed by benzene, generating low energy  
 198 photoelectrons that can react with CH<sub>3</sub>I to produce I<sup>-</sup> (Ji et al., 2020). The I<sup>-</sup> reacts with analytes for approximately 30 ms  
 199 before being drawn through another critical orifice where the sample travels through four differentially pumped chambers  
 200 before reaching the drift region of the ToF-CIMS. Ions in the ToF chamber are extracted and converted into mass spectra via  
 201 an MCP detector with a preamplifier over a mass range of 7-510 Th. The extracted packets are averaged over a period of 1  
 202 second and the resolution of the instrument is ≈ 5000. Data was collected at a rate of 1 Hz. Data averaging, mass calibration,  
 203 peak assignment, peak fitting and peak integration are all performed using the software package Tofware (version 4.0.0,  
 204 TOFWERK) used in Igor Pro 9 software (Wavemetrics). Peak fitting focused on I<sup>35</sup>ClNO<sub>2</sub><sup>-</sup> (m/z 207.8668) and I<sup>37</sup>ClNO<sub>2</sub><sup>-</sup> (m/z  
 205 209.8638), and isotope abundances were manually confirmed to be ~1:0.32, based on the natural abundance of chlorine  
 206 isotopes. CIMS signals were normalized against the sum of the total number of reagent ions, which is equivalent to I<sup>-</sup> + I(H<sub>2</sub>O)<sup>-</sup>  
 207 . Additionally, as the CIMS sensitivity to ClNO<sub>2</sub> varies with humidity in the ion-molecule reactor region, we define an  
 208 additional term equal to ratio of the iodide water cluster (I(H<sub>2</sub>O)<sup>-</sup>) to the reagent ion sum (I<sup>-</sup> + I(H<sub>2</sub>O)<sup>-</sup>), hereafter referred to as  
 209 the Iodide Water Ratio (IWR). Instrument backgrounds were assessed using air scrubbed of ClNO<sub>2</sub>, as described in Sect. 2.2.



## 210 2.4 Data Analysis

211 Data analysis was conducted using the R language for statistical computing (R Core Team, 2021). Linear regressions were  
212 calculated using the York method (Cantrell, 2008) when possible so as to incorporate uncertainties in compared variables.

## 213 2.5 Chemical Modelling

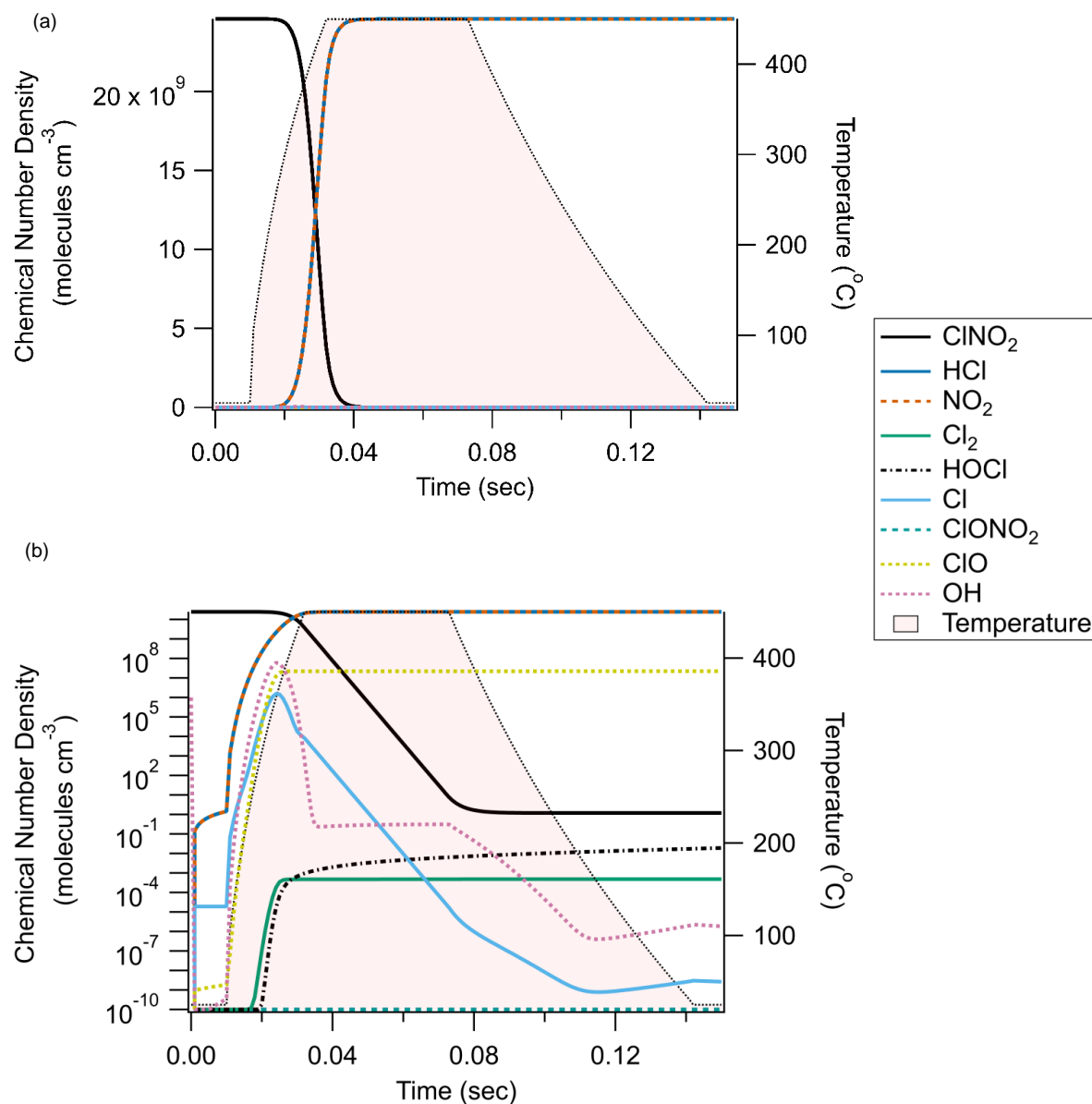
214 The 0-D box model Kintecus (Ianni, 2003, 2022) was used to predict the timescales for the thermal-dissociation of  $\text{ClNO}_2$  and  
215 the subsequent formation of HCl after reaction with hydrocarbons (Reaction R2), as well as to identify potential interferents  
216 that could prevent unit conversion of  $\text{ClNO}_2$  to HCl. The results of the model were used to guide the experimental set-up. The  
217 modelled species, reaction list, and initial concentrations are included in the Appendix (Tables A1-A3). Reaction kinetics were  
218 sourced from the NIST Chemical Kinetics Database and IUPAC Evaluated Kinetic Data websites (Manion et al., 2015;  
219 Wallington et al., 2021), and primary literature references are listed next to each reaction. The model integration time was set  
220 to 1 ms, and the entire simulation was set to last 150 ms. The model initiated with a temperature of 25 °C (held for 10 ms)  
221 before increasing to 450 °C over the course of 22 ms. The temperature was held at 450 °C for 40 ms, before gradually decaying  
222 back to 25 °C over 70 ms.

## 223 3 Results & Discussion

### 224 3.1 Modelling TD Chemistry

225 Box model simulations predicted the rapid, virtually unit conversion of  $\text{ClNO}_2$  to HCl after increasing temperature to 450 °C  
226 (Fig. 2). Ninety percent conversion was calculated to occur within 23 ms from a starting  $\text{ClNO}_2$  concentration of  $2.46 \times 10^{10}$   
227 molecules  $\text{cm}^{-3}$  (1 ppbv at 25 °C), and ambient mixing ratios of methane (i.e., 2 ppbv at 25°C) were found to be sufficient for  
228 facilitating this chemistry. While Cl-mediated hydrocarbon oxidation was shown to produce a modest enhancement of  
229 hydroxyl radical concentrations (Fig. 2b), it was not enough to compete meaningfully with Cl to mitigate or retard Reaction  
230 R1. Similarly, an initial  $\text{O}_3$  concentration of  $9.84 \times 10^{11}$  molecules  $\text{cm}^{-3}$  (40 ppbv at 25°C) did not significantly inhibit the  
231 desired chemistry by the direct reaction of  $\text{O}_3$  with Cl radicals.

232



233 **Figure 2: Chemical modelling results of the thermal dissociation of  $\text{ClNO}_2$  and its subsequent conversion to  $\text{HCl}$ .**  
 234 **Panel A presents results on a linear y-axis, while Panel B features the same data on a logarithmic y-axis.**

235 Concerning potential interferents,  $\text{ClNO}_2$  was predicted to be the only source of inorganic chlorine to thermally dissociate at  
 236 450  $^{\circ}\text{C}$ . This is consistent with the relative bond dissociation energies found for  $\text{ClNO}_2$  ( $142 \text{ kJ mol}^{-1}$ ) relative to the various  
 237 other forms of inorganic chlorine simulated ( $\text{Cl-NO}_2 < \text{Cl-Cl} < \text{Cl-O} < \text{Cl-R} < \text{Cl-H}$ ) (Darwent, 1970). Finally, production of  
 238 other inorganic chlorine compounds (e.g.,  $\text{Cl}_2$ ,  $\text{HOCl}$ ,  $\text{ClONO}_2$ , or reformation of  $\text{ClNO}_2$ ) was orders of magnitude less than  
 239 the resulting  $\text{HCl}$  and is therefore not believed to influence  $\text{HCl}$  production. One notable class of compounds that could not be





simulated were chloramines, which have recently received increased attention as relevant daytime sources of Cl atoms (A. Angelucci et al., 2023; Wang et al., 2023). Trichloramine, dichloramine, and monochloramine have reported bond dissociation energies of 381, 280, 251 kJ mol<sup>-1</sup>, respectively (Darwent, 1970), and so would not be expected to produce free Cl radicals in the temperature range simulated herein if its thermochemistry is consistent with the above bond dissociation energy trend. However, to the authors' knowledge no information is available regarding its thermal stability in the gas phase at atmospherically relevant conditions, and this potential source of positive interference for our proposed method cannot be discounted via the model at this time.

### 3.2 Laboratory Characterization of TD-TILDAS

For laboratory characterization, a stable source of ClNO<sub>2</sub> was generated (Sect. 2.1) for assessing TD-TILDAS performance in comparison with other established ClNO<sub>2</sub> sampling techniques, including CAPS NO<sub>2</sub> and CIMS (Sect. 2.3). One key change between model simulations and this experimental setup is the inclusion of propane to the sample stream (estimated mixing ratio of 5 ppmv within the heated section of sample configuration). While the model predicted the pertinent chemistry will occur in ~23 ms using only ambient methane as the hydrocarbon (Sect. 3.1) and the residence time in the heated furnace is ~500 ms, adding propane ensures complete conversion of ClNO<sub>2</sub> to HCl and ensures wall losses are negligible, as Cl radicals react with propane approximately 3 orders of magnitude faster than with methane (Atkinson et al., 2006a). The fact that no additional HCl signal was observed on addition of propane at varying levels (not shown) supports our calculations that unit conversion is achieved and competitive loss of Cl radicals to walls is negligible.

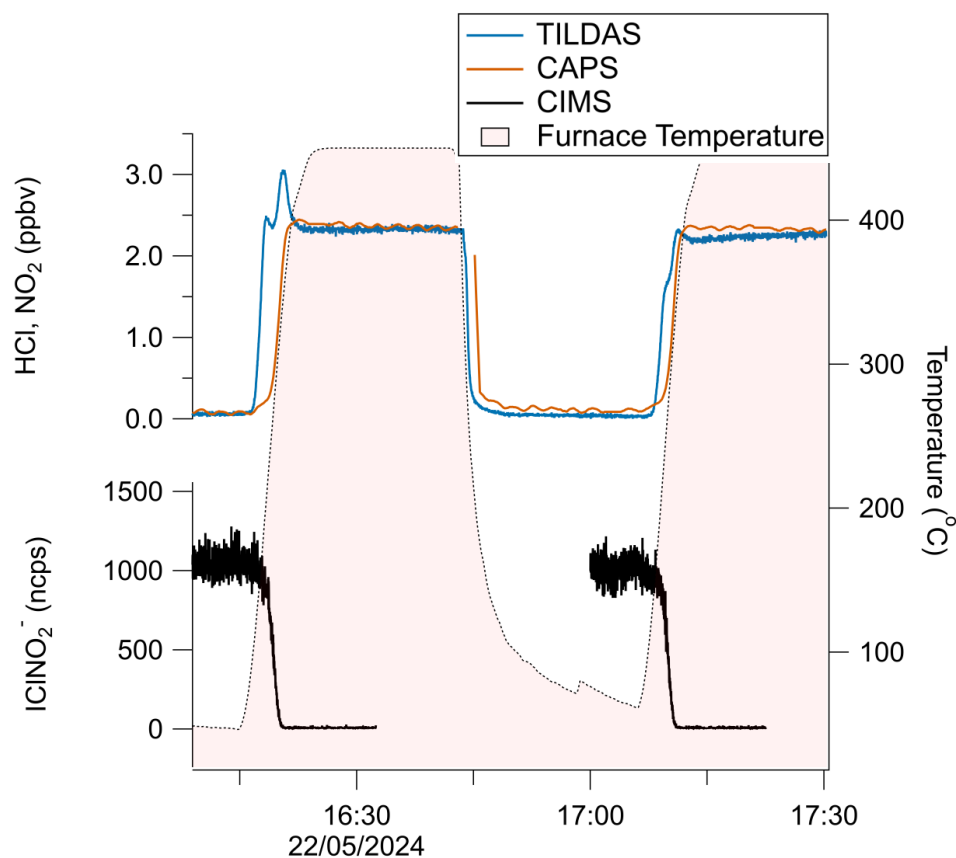
A schematic diagram of these experiments is shown in Fig. 1a. Figure 3 represents a typical comparison experiment in which ClNO<sub>2</sub> was sampled by all three instruments simultaneously. First, ClNO<sub>2</sub> was introduced into the flow stream with the furnace unheated, yielding a positive CIMS signal for ICINO<sub>2</sub><sup>+</sup> (~1100 ncps for the example in Fig. 3), while TILDAS HCl and CAPS NO<sub>2</sub> mixing ratios remained at background levels. As the furnace temperature approached 450 °C, Reactions R1-R2 began to occur. HCl and NO<sub>2</sub> mixing ratios rose, plateauing at similar values (~2.2 ppbv in Fig. 3) while ICINO<sub>2</sub><sup>+</sup> decreased to the instrument baseline, implying both Reactions R1-R2 proceeded to completion. Signals returned to their original positions once the furnace was allowed to cool back to room temperature (e.g., from 16:45 in Fig. 3). Note that HCl signal spike during the furnace's temperature ramp was seen consistently across experiments, and was most likely caused by a shift in HCl molecule partitioning between the surface of the quartz tubing toward the gas phase (Halfacre et al., 2023). Allan-Werle deviation calculations demonstrate favourable performance metrics for TILDAS while sampling ClNO<sub>2</sub>, with 1 Hz precision of 11.8 pptv, and as good as 1.2 pptv with an integration time of 96 seconds (Fig. 4).

A summary of comparison experiments across varied humidities is presented in Fig. 5. The changes in HCl as observed by TILDAS correlated strongly with the changes in NO<sub>2</sub> observed by the CAPS instrument (Pearson correlation coefficients of 0.999, 0.997, and 0.987 for relative humidities of 11%, 44%, and 66%, respectively). However, the slopes were consistently less than unity ( $0.95 \pm 0.01$ ,  $0.93 \pm 0.02$ , and  $0.91 \pm 0.02$  at 11%, 44%, and 66%, respectively), indicating observed HCl mixing ratios were less than corresponding NO<sub>2</sub> mixing ratios. One potential explanation for this could be loss of Cl radical loss in the furnace, but we do not believe this to be the case (as detailed above). While physical losses of HCl to sampling lines would not be unexpected as HCl has a high affinity for sorbing to physical surfaces, experiments were designed to minimize these interactions, and line loss experiments were performed to quantify any losses observed at tested humidities. Experimentally, a small flow (50-75 mL min<sup>-1</sup>) of PFBS vapour was injected into the TILDAS sampling line downstream of the furnace to reduce HCl affinity for surfaces (Sect. 2.2) (Note that PFBS was not introduced to the entirety of the flow path to avoid sampling of PFBS by other instruments. Additionally, there is evidence that PFBS degrades at temperatures above 400°C (Xiao et al., 2020), and so its ultimately efficacy and reproducibility within the furnace system would be uncertain).



Further, the high operating temperature of the furnace would also be expected to minimize HCl-wall interactions within the quartz tubing. Indeed, no line losses were found at 11% relative humidity between when the HCl permeation source standard was injected into the sampling line before the furnace ( $2.95 \pm 0.02$  ppbv) and when HCl was injected just before the inertial inlet (accounting for dilution factors) ( $2.95 \pm 0.02$  ppbv), consistent with Halfacre et al. (2023). Similar results were found at 44% relative humidity (pre-furnace value of  $2.68 \pm 0.03$  ppbv vs  $2.66 \pm 0.03$  ppbv when HCl was introduced at inlet), and real HCl loss was quantified at 66% relative humidity (pre-furnace value of  $1.87 \pm 0.03$  ppbv vs  $1.97 \pm 0.03$  ppbv when HCl introduced at inlet). Having accounted for these line losses, ANOVA calculations found no significant differences between these three slopes as presented in Fig. 3 ( $F(2,19) = 0.10$ ,  $p = 0.902$ ), indicating consistent performance between TILDAS and CAPS for detecting  $\text{ClNO}_2$ . However, it does not appear to explain the deviation from unity, which will be discussed below.

As discussed in Sect. 2.1, chemistry may occur within the slurry to produce  $\text{N}_2\text{O}_4$ , which can easily degrade at room temperature to produce two  $\text{NO}_2$  molecules. If the  $\text{N}_2\text{O}_4$  output from the  $\text{NO}_2/\text{Cl}^-$  slurry is constant over the timescale of an experiment ( $< 1$  hr), it would be expected this additional  $\text{NO}_2$  is readily accounted for during blank subtraction calculations. While we believe this is largely true for the experiments presented above, discrepancies in  $\text{ClNO}_2$  signals were observed as the slurry aged ( $> \sim 3$  weeks), with CAPS-observed  $\text{NO}_2$  mixing ratios growing in significant excess of TILDAS-observed HCl mixing ratios (Fig. A2). Separate applications of TILDAS- and CAPS-based calibration factors (using data from Fig. 5) to concurrent CIMS  $\text{ClNO}_2$  observations show closer resemblance to the TILDAS-observed mixing ratios (Fig. A2), suggesting additional chemistry may be occurring within the salt bed that produces stable reservoirs of  $\text{NO}_2$  that thermally dissociate in the furnace to produce undesired  $\text{NO}_2$ . This  $\text{NO}_2$  artefact serves as a likely explanation for the sub-unity slopes presented in Fig. 5, as it would positively bias the CAPS measurements but not the TILDAS, which is only sensitive to HCl. We are not aware of such chemistry being addressed in the literature for this  $\text{ClNO}_2$  generation method and do not propose potential reactions as it is outside the scope of this paper.



301  
 302 **Figure 3: a) Time series demonstrating the reversible thermal conversion of  $\text{ClNO}_2$  to  $\text{NO}_2$  (red trace, CAPS) and HCl (blue trace,**  
 303 **TILDAS), as evidenced by changes in CIMS-observed  $\text{IClNO}_2^-$  (black). Gaps in CIMS data are from internal CIMS tests not**  
 304 **pertinent to this work.**

305 Both HCl and  $\text{NO}_2$  mixing ratios independently correlated strongly with the CIMS measurement of  $\text{IClNO}_2^-$  (Fig. 5b,  
 306 c), and the I<sup>-</sup> CIMS sensitivity for  $\text{IClNO}_2^-$  was found to vary strongly with humidity, as previously reported (Kercher et al.,  
 307 2009; Mielke et al., 2011). The weakest Pearson correlation coefficient was for  $\text{NO}_2$  and  $\text{IClNO}_2^-$  at 66% relative humidity ( $r$   
 308  $= 0.988$ ), virtually matching that of  $\text{NO}_2^-$  and HCl at the same humidity. Due to the uncertainty / unreliability of the  $\text{NO}_2$  as it  
 309 relates to  $\text{ClNO}_2$  quantitation, we do not further consider the relationship between CAPS and CIMS.

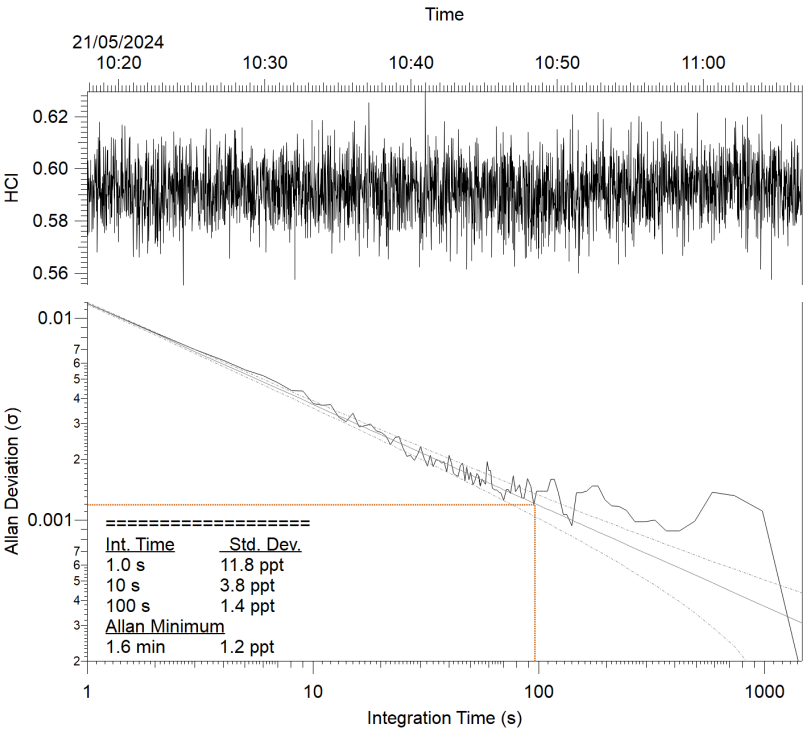
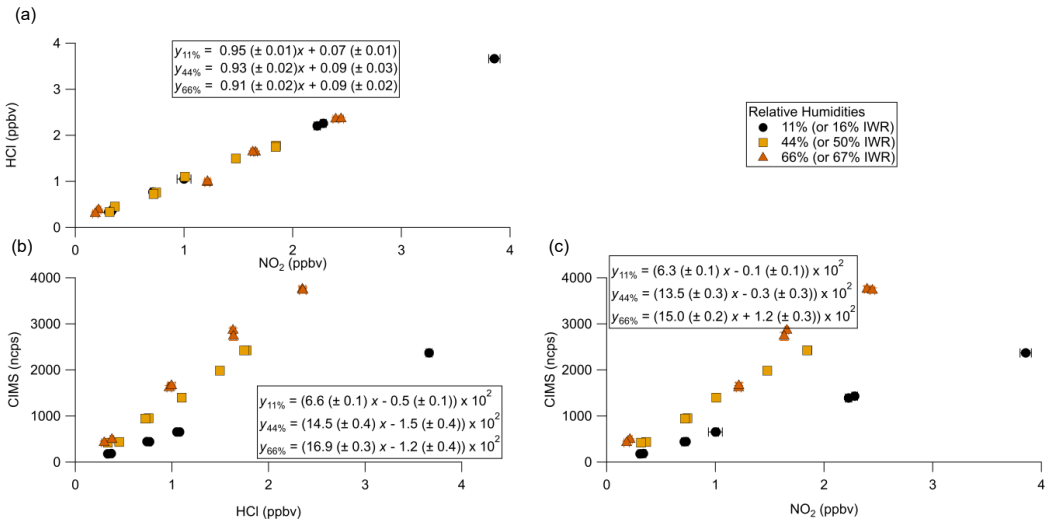


Figure 4: Allan-Werle plot for TD-TILDAS during addition of  $\text{ClNO}_2$  standard into the sample line. The Allan minimum is indicated by the dotted red lines.





**Figure 5 – Comparison curves of a) TILDAS vs CAPS, b) CIMS vs TILDAS, and c) CIMS vs CAPS for injections of varied mixing ratios of ClNO<sub>2</sub> across different relative humidities. Regressions involving TILDAS data have been corrected for line losses observed at 66% relative humidity.**

The linear equations from Fig. 5a present significant intercepts that suggest a source of positive error for the TILDAS, and the similarity of these intercepts suggest a relatively constant/consistent source (values are statistically the same  $F(4,19) = 0.624$ ,  $p = 0.546$  per ANOVA). For these experiments, TILDAS blanks were obtained by sampling slurry air flowed through an unheated furnace; in this scenario, Reactions R1-R2 are unable to occur, and therefore any signal observed by TILDAS could be considered background. It is possible that a small amount of HCl forms in the slurry system from the aqueous disproportion reaction between Cl<sub>2</sub> and H<sub>2</sub>O. When the furnace is unheated, some amount of HCl interaction with the quartz tubing is expected given there is no PFBS flow through this portion of the plumbing, biasing this blank measurement low. Then, once the furnace is heated to 450 °C, this HCl will be liberated from the quartz tubing, possibly then biasing the heated measurement high. This is supported by the presence of a peak in observed HCl as the furnace reheats (e.g., as in the second temperature ramp in Fig. 3), as some of the HCl sorbed to the furnace tube walls under room temperature is forced into the gas phase. The statistical similarity in intercepts implies this effect is constant across these experiments, leading to a consistent offset. While an ideal blank would sample the gas downstream of the slurry while selectively scrubbing ClNO<sub>2</sub>, this was not practical to achieve without simultaneously scrubbing HCl. Therefore, we propose the y-intercept in these cases is a good estimate of the systematic error present in these comparison experiments.

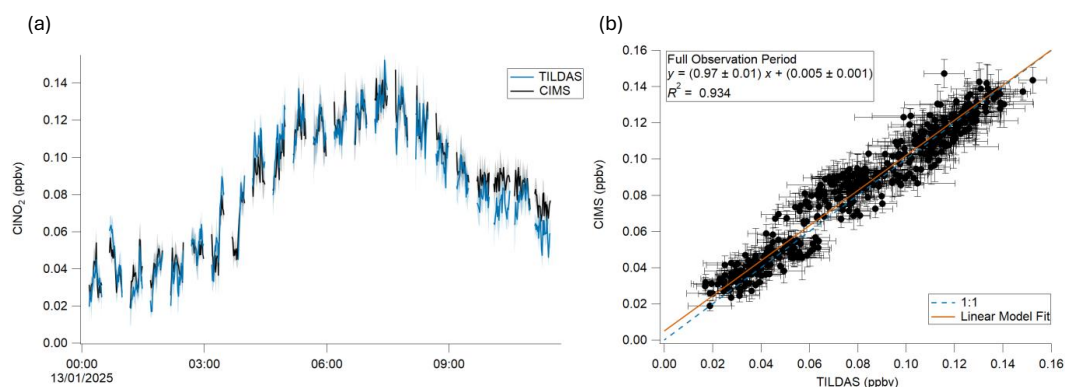
### 3.3 Applicability as Field Instrument

The applicability of TD-TILDAS as a field method for ClNO<sub>2</sub> detection was tested by sampling ambient air from outside the Wolfson Atmospheric Chemistry Laboratory building on the University of York campus (York, United Kingdom) from the morning of 13 January 2025 (Fig. 6). Compared with the laboratory-based configuration described in Sect. 3.2, ambient air will contain varied amounts of HCl that would interfere with accurate quantification of ClNO<sub>2</sub> via the TILDAS method. To address this, a base-coated denuder (Sect. 2.2) was installed in the HCl sampling line. ClNO<sub>2</sub> throughput was found to be hindered when flowed through the denuder but increased over the course of the observation period (pre-experiment estimation of 55% loss vs 31% measured directly after the experiment). This loss was accounted for by applying a time-varying, linearly interpolated correction factor for the denuder. In addition, line losses affecting HCl between the heated furnace and TILDAS inlet were estimated as 2.7%, which was added back into the TILDAS measurements. CIMS observations of ICINO<sub>2</sub><sup>-</sup> were calibrated against TD-TILDAS using a mid-experiment ClNO<sub>2</sub> addition, yielding a sensitivity factor of 1982 ncps ppb<sup>-1</sup> (measured with a corresponding IWR of 42%). We note that this factor is ~35% greater than the value of 1450 ncps ppbv<sup>-1</sup> as presented in Fig. 5b for a comparable IWR (44%); this is likely due to the replacement of the reagent ion permeation source and change in CIMS inlet configuration between the experiments from Sect. 3.2 and this section. Application of this sensitivity factor across this measurement period can be justified as the IWR was found to be stable ( $38 \pm 2\%$ ). Limits of detection, based on instrument blanks, were found to average  $10 \pm 5$  pptv for TD-TILDAS and  $1 \pm 1$  pptv for CIMS (using 60 second data averaging).

As seen in Fig. 6a, TILDAS- and CIMS-observed ClNO<sub>2</sub> demonstrate very good agreement for these ambient observations in both signal magnitude and structure. This is quantitatively supported by regression calculations during this period that yield a slope of  $0.97 \pm 0.01$  (Fig. 6b), which is well within the averaged combined uncertainty for this period of 9%. While the sub-unity slope could indicate small losses on the TILDAS method, pre- and post-experimental losses were tested and corrected for as detailed above, and so this is not believed to be a large source of error in this case. It is otherwise not unexpected that this slope is found to deviate from unity given the uncertainty in the application of a single-point CIMS



353 sensitivity factor. Nevertheless, this agreement gives us confidence that it is appropriate for these measurements and provides  
 354 proof-of-concept for this TILDAS method.  
 355



356  
 357 **Figure 6 – a) Time series comparison of TILDAS and CIMS observations of  $\text{ClNO}_2$ . b) Scatter plot of data shown in panel (a). The**  
 358 **error shading in (a) and bars in (b) represent the standard deviation of the 60 s averaged measurements.**

359 Additional sources of measurement uncertainty include unaccounted-for thermolabile chlorine reservoirs that could  
 360 cause positive interference in the TILDAS-method. As stated above, the TD-TILDAS method functions on the assumption  
 361 that  $\text{ClNO}_2$  is the only inorganic chlorine source that thermally dissociates at 450 °C. However, relevant thermochemistry  
 362 information is unavailable for chloramines, which therefore cannot be ruled out as possible interferences. Indeed, while CIMS  
 363 signals of chloramines did not rise above their baselines during the period shown in Fig. 6, a separate measurement period  
 364 demonstrates multiple occurrences where signal increases in iodide-tri- and di-chloramine adducts ( $\text{INCl}_3^-$ ,  $\text{INHCl}_2^-$ )  
 365 correspond with TILDAS-observed signal increases (Fig. A3). This is most dramatic at ~08:15, where ~115 ncps of  $\text{INCl}_3^-$   
 366 and 18 ncps of  $\text{INHCl}_2^-$  corresponds with an increase of 100 pptv in the TILDAS signal. Synthesis and calibration of chloramine  
 367 standards is a non-trivial task (Wang et al., 2023), and so further experiments are required to investigate 1) to what extent the  
 368 chloramine signals can be quantified by TILDAS and 2) if the chloramine signal can be dissected from the  $\text{ClNO}_2$  signal  
 369 through temperature scans. The results of such experiments may therefore allow this method to be extended for the  
 370 quantification of both chloramines and  $\text{ClNO}_2$ .

## 371 Conclusions

372 This work demonstrates the viability of TD-TILDAS as an independent  $\text{ClNO}_2$  detection method at performance metrics  
 373 comparable to quadrupole CIMS, which are more than adequate for commonly observed mixing ratios in the boundary layer.  
 374 While modern CIMS instruments can achieve lower limits of detection and higher precision, the major advantage of TD-  
 375 TILDAS over CIMS is that it does not require external  $\text{ClNO}_2$  calibration experiments, as this work demonstrates the unity  
 376 conversion of  $\text{ClNO}_2$  to  $\text{HCl}$  that is subsequently detected based on well-understood spectroscopic principles. The TD method  
 377 described here can thus be used effectively in laboratory settings to measure  $\text{ClNO}_2$  in related experiments, or even to calibrate  
 378 CIMS for  $\text{ClNO}_2$  directly without needing to make assumptions regarding  $\text{Cl}_2$  conversion on salt slurries. Additionally, use of  
 379 a denuder allows this method to be readily applied to other  $\text{HCl}$  optical instruments, such as those based on CRDS.



380           As a field method, TD-TILDAS demonstrated excellent agreement with a co-located CIMS for ClNO<sub>2</sub> detection.  
381   However, the TD-TILDAS method appears susceptible to positive interference, potentially resulting from chloramines or other  
382   unaccounted-for thermolysable chlorine compounds. More work is required to confirm and quantify the response of this  
383   method to chloramines, and if so, identify an appropriate method to mitigate this potential interference. Experimental  
384   adjustments could be further made for the TILDAS to alternate its sampling between a heated channel (as described in this  
385   paper) for ClNO<sub>2</sub> detection and an unheated pathway that allows for the additional detection of HCl. Doing so would require  
386   careful characterization of physical HCl losses inherent to both sampling pathways, as well as consideration of the likely  
387   hysteresis in detected HCl mixing ratios resulting from changes to the sampled air temperature that would affect the partitioning  
388   of HCl between surfaces and the gas phase.  
389  
390



391 **Appendix 1**

392 **Table A1 – Bimolecular reactions and parameters used for the modelling described in Sect. 2.5. Reactions follow the rate expression**  
 393  $k(T) = A (T/298)^n e^{-E_a/RT}$  (Burkholder et al., 2015)

Reaction	A	n	E <sub>a</sub> (kJ mol <sup>-1</sup> )	Reference
ClNO <sub>2</sub> + M ==> Cl + NO <sub>2</sub>	9.13 x 10 <sup>-10</sup>	0	106	(Baulch et al., 1981)
Cl + Cl ==> Cl <sub>2</sub>	6.15 x 10 <sup>-34</sup>	0	-7.53	(Baulch et al., 1981)
M + ClONO <sub>2</sub> ==> NO <sub>2</sub> + ClO	2.76 x 10 <sup>-5</sup>	0	94.78	(Anderson and Fahey, 1990)
CH <sub>4</sub> + Cl ==> CH <sub>3</sub> + HCl	8.24 x 10 <sup>-13</sup>	2.49	5.06	(Bryukov et al., 2002)
HCl + OH ==> H <sub>2</sub> O + Cl	3.74 x 10 <sup>-12</sup>	0	4.27	(Baulch et al., 1981)
HCl + M ==> H + Cl	7.31 x 10 <sup>-11</sup>	0	342	(Baulch et al., 1981)
CH <sub>3</sub> + HCl ==> CH <sub>4</sub> + Cl	3.89 x 10 <sup>-13</sup>	0	9.64	(Baulch et al., 1981)
CH <sub>3</sub> + NO <sub>2</sub> ==> CH <sub>3</sub> O + NO	3.44 x 10 <sup>-11</sup>	0	0	(Srinivasan et al., 2005)
O <sub>3</sub> + M ==> O + O <sub>2</sub>	7.6 x 10 <sup>-10</sup>	0	93.12	(Heimerl and Coffee, 1979)
CH <sub>3</sub> + O ==> CH <sub>2</sub> O + H	2.26 x 10 <sup>-11</sup>	0	0	(Baulch et al., 1992)
HCl + O ==> OH + Cl	7.07 x 10 <sup>-14</sup>	2.87	14.72	(Mahmud et al., 1990)
OH + CH <sub>4</sub> ==> CH <sub>3</sub> + H <sub>2</sub> O	4.16 x 10 <sup>-13</sup>	2.18	10.24	(Srinivasan et al., 2005)
Cl <sub>2</sub> + M ==> Cl + Cl	3.85 x 10 <sup>-11</sup>	0	196	(Baulch et al., 1981)
Cl + Cl ==> Cl <sub>2</sub>	6.15 x 10 <sup>-34</sup>	0	-7.53	(Baulch et al., 1981)
Cl <sub>2</sub> + O ==> ClO + Cl	4.17 x 10 <sup>-12</sup>	0	11.39	(Baulch et al., 1981)
Cl <sub>2</sub> + H ==> HCl + Cl	1.43 x 10 <sup>-10</sup>	0	4.91	(Baulch et al., 1981)
Cl <sub>2</sub> + OH ==> HOCl + Cl	3.60 x 10 <sup>-12</sup>	0	9.98	(Atkinson et al., 2007)
CH <sub>3</sub> + O <sub>2</sub> ==> CH <sub>3</sub> O + O	2.19 x 10 <sup>-10</sup>	0	131	(Baulch et al., 1992)





$\text{ClO} + \text{O} \Rightarrow \text{O}_2 + \text{Cl}$	$2.50 \times 10^{-11}$	0	-0.91	(Atkinson et al., 2007)
$\text{OH} + \text{ClO} \Rightarrow \text{HO}_2 + \text{Cl}$	$6.86 \times 10^{-12}$	0	-2.49	(Atkinson et al., 2007)
$\text{OH} + \text{ClO} \Rightarrow \text{HCl} + \text{O}_2$	$4.38 \times 10^{-13}$	0	-2.49	(Atkinson et al., 2007)
$\text{CH}_3\text{O} + \text{NO} \Rightarrow \text{CH}_2\text{O} + \text{HNO}$	$4.00 \times 10^{-12}$	-0.7	0	(Atkinson et al., 1992)
$\text{CH}_3\text{O} + \text{O}_2 \Rightarrow \text{CH}_2\text{O} + \text{HO}_2$	$7.20 \times 10^{-14}$	0	8.98	(Atkinson et al., 1992)
$\text{HOCl} + \text{O} \Rightarrow \text{OH} + \text{ClO}$	$1.70 \times 10^{-13}$	0	0	(Atkinson et al., 2007)
$\text{ClCO} + \text{M} \Rightarrow \text{CO} + \text{Cl}$	$4.10 \times 10^{-10}$	0	24.6	(Atkinson et al., 2007)
$\text{O}_3 + \text{NO} \Rightarrow \text{O}_2 + \text{NO}_2$	$1.40 \times 10^{-12}$	0	10.9	(Atkinson et al., 2004)
$\text{CH}_3\text{O}_2 + \text{NO} \Rightarrow \text{CH}_3\text{O} + \text{NO}_2$	$2.30 \times 10^{-12}$	0	-2.99	(Atkinson et al., 2006b)
$\text{HO}_2 + \text{NO} \Rightarrow \text{NO}_2 + \text{OH}$	$3.6 \times 10^{-12}$	0	-2.24	(Atkinson et al., 2004)
$\text{CH}_2\text{O} + \text{Cl} \Rightarrow \text{HCl} + \text{HCO}$	$8.20 \times 10^{-11}$	0	0.28	(Atkinson et al., 1992)
$\text{CH}_2\text{O} + \text{OH} \Rightarrow \text{HCO} + \text{H}_2\text{O}$	$4.73 \times 10^{-12}$	1.18	-1.87	(Baulch et al., 1992)
$\text{CH}_3\text{O}_2 + \text{HO}_2 \Rightarrow \text{CH}_3\text{OOH} + \text{O}_2$	$3.80 \times 10^{-13}$	0	-6.49	(Atkinson et al., 1992)
$\text{CH}_3\text{OOH} \Rightarrow \text{CH}_3\text{O} + \text{OH}$	$6.00 \times 10^{14}$	0	177	(Baulch et al., 1994)
$\text{HCO} + \text{O}_2 \Rightarrow \text{CO} + \text{HO}_2$	$5.20 \times 10^{-12}$	0	0	(Atkinson et al., 2006b)
$\text{CO} + \text{OH} \Rightarrow \text{CO}_2 + \text{H}$	$5.40 \times 10^{-14}$	1.5	-2.08	(Baulch et al., 1992)
$\text{Cl} + \text{HO}_2 \Rightarrow \text{HCl} + \text{O}_2$	$1.80 \times 10^{-11}$	0	-1.41	(Atkinson et al., 1992)
$\text{Cl} + \text{HO}_2 \Rightarrow \text{ClO} + \text{OH}$	$6.30 \times 10^{-11}$	0	4.74	(Atkinson et al., 2007)



$\text{Cl} + \text{O}_3 \Rightarrow \text{ClO} + \text{O}_2$	$2.80 \times 10^{-11}$	0	2.08	(Atkinson et al., 2007)
$\text{CO} + \text{Cl} \Rightarrow \text{ClCO}$	$1.33 \times 10^{-33}$	-3.8	0.00	(Atkinson et al., 2007)
$\text{OH} + \text{HOCl} \Rightarrow \text{H}_2\text{O} + \text{ClO}$	$5.00 \times 10^{-13}$	0	0	(Atkinson et al., 2007)
$\text{ClO} + \text{HO}_2 \Rightarrow \text{HOCl} + \text{O}_2$	$2.20 \times 10^{-12}$	0	-2.8	(Atkinson et al., 2007)
$\text{ClO} + \text{ClO} \Rightarrow \text{Cl}_2 + \text{O}_2$	$1.00 \times 10^{-12}$	0	13.22	(Atkinson et al., 2007)
$\text{ClO} + \text{ClO} \Rightarrow \text{OCIO} + \text{Cl}$	$3.50 \times 10^{-13}$	0	11.39	(Atkinson et al., 2007)
$\text{ClO} + \text{ClO} \Rightarrow \text{ClOO} + \text{Cl}$	$3.00 \times 10^{-11}$	0	20.37	(Atkinson et al., 2007)
$\text{ClO} + \text{NO} \Rightarrow \text{Cl} + \text{NO}_2$	$6.20 \times 10^{-12}$	0	-2.45	(Atkinson et al., 2007)
$\text{CH}_2\text{O} + \text{O} \Rightarrow \text{HCO} + \text{OH}$	$1.78 \times 10^{-11}$	0.57	11.56	(Baulch et al., 1992)
$\text{OH} + \text{NO}_2 \Rightarrow \text{HNO}_3$	$2.70 \times 10^{-11}$	0	0	(Troe, 2012)

394

395



**Table A2 – Termolecular reactions and parameters used for the modelling described in Sect. 2.5. The effective rate constant is calculated by combining the low- and high-pressure limit expressions into the following formula:  $k_f(T, [M]) =$**

**$\frac{k_{\infty}(T)k_0(T)[M]}{k_{\infty}(T) + k_0(T)[M]} \cdot 0.6^{\{1 + \log_{10}(\frac{k_0(T)[M]}{k_{\infty}(T)})^2\}^{-1}}$**

Reaction	Low-Pressure Limit $k_0 = k_0^{298}(T/298)^{-n}$		High Pressure Limit $k_{\infty} = k_{\infty}^{298}(T/298)^{-m}$		Reference
	$k_0^{298}$	n	$k_{\infty}^{298}$	m	
$\text{Cl} + \text{NO}_2 + \text{M} \Rightarrow \text{ClNO}_2 + \text{M}$	$1.8 \times 10^{-31}$	2	$1.1 \times 10^{-10}$	1	(Burkholder et al., 2015)
$\text{CH}_3 + \text{O}_2 + \text{M} \Rightarrow \text{CH}_3\text{O}_2 + \text{M}$	$4.1 \times 10^{-31}$	3.6	$1.2 \times 10^{-12}$	-1.1	(Burkholder et al., 2015)



402 **Table A3 – Initial concentrations for specified species simulated in model. All other compounds were initialised with a concentration**  
 403 **of 0 molecules cm<sup>-3</sup>.**

Species	Initial Concentration (molecules cm <sup>-3</sup> )
ClNO <sub>2</sub>	2.46 x 10 <sup>10</sup> (1 ppbv)
N <sub>2</sub>	1.92 x 10 <sup>19</sup> (78%)
O <sub>2</sub>	5.17 x 10 <sup>19</sup> (21%)
CH <sub>4</sub>	4.92 x 10 <sup>13</sup> (2 ppmv)
OH	1 x 10 <sup>6</sup>
O <sub>3</sub>	9.84 x 10 <sup>11</sup> (40 ppbv)

404

405

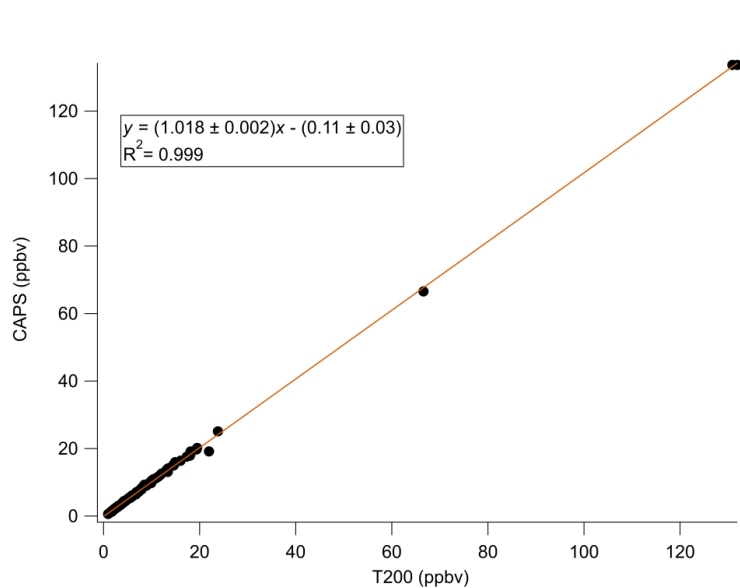
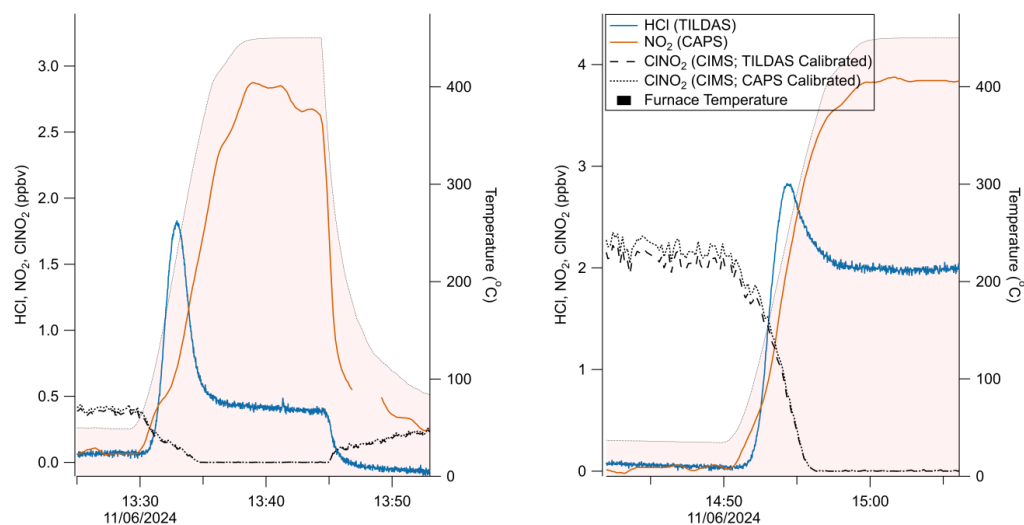


**Figure A1 – Laboratory calibration curve for CAPS NO<sub>2</sub>**



411



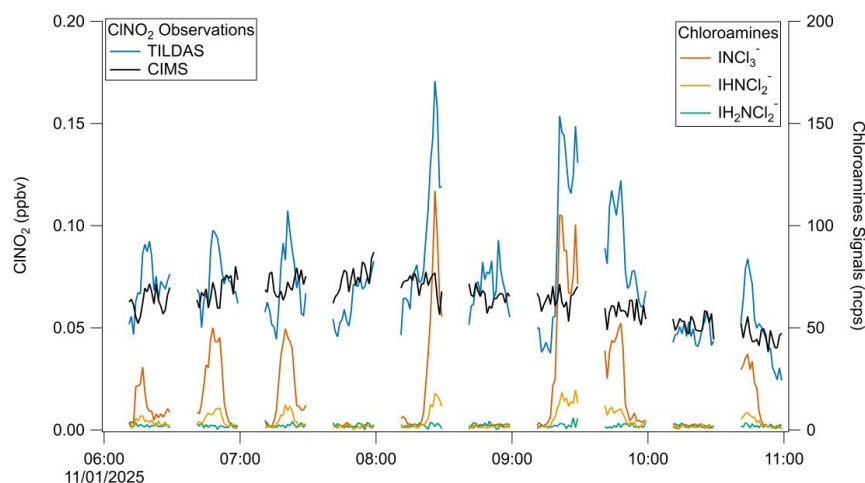
412

413 **Figure A2 – a) Comparison plot of  $\text{ClNO}_2$  observations with an apparent excess of  $\text{NO}_2$  formed after aging/processing of the same**  
 414 **slurry used for generating Fig. 3-4. (b) Additional comparison using a freshly made slurry. CIMS signal was calibrated**  
 415 **humidity-dependent calibration factors as presented in Fig. 5.**

416



417



418

419 **Figure A3 –Field data showing apparent coincident signal increases TILDAS-observed  $\text{ClNO}_2$  with CIMS-observed chloramines**  
 420 **(uncalibrated).**

#### 421 **Code availability**

422 Code used for this analysis is available from the corresponding author on request.

#### 423 **Data availability**

424 Data are available from the corresponding author on request.

#### 425 **Author contribution**

426 PRV, MAR, SSB designed and performed proof-of-concept experiments to demonstrate potential of the method.  
 427 SCH, HRR, CD, TIY designed, built, and tested the HCl TILDAS at Aerodyne Research, Inc. SCH, HRR, CD, TIY, and PME  
 428 designed initial laboratory experiments.  
 429 JWH and PME designed laboratory and field experiments, and JWH conducted laboratory and field experiments presented in  
 430 this work.  
 431 LM, MDS, LJC provided support for laboratory use of CIMS. EM, TJB, HC provided support for field CIMS observations.  
 432 JWH prepared the manuscript, and all authors reviewed the manuscript.

433

#### 434 **Competing interests**

435 The authors declare that they have no conflicts of interest.



## 436 Acknowledgements

437 The authors would also like to thank Abigail Mortimer for her glassblowing services, Stephen Andrews and Stuart Young for  
 438 assistance with creating custom furnaces. Additionally, the authors thank William Drysdale and Katie Read for assistance with  
 439 calibrating and using the York CAPS instrument. Further, the authors thank Michael Agnese and Michael Moore for TILDAS  
 440 technical support.

## 442 Financial Support

443 This research has been supported by the European Research Council (H2020, grant no. ERC-StG 802685).

## 444 References

- 445 A. Angelucci, A., R. Crilley, L., Richardson, R., E. Valkenburg, T. S., S. Monks, P., M. Roberts, J., Sommariva, R., and  
 446 C. VandenBoer, T.: Elevated levels of chloramines and chlorine detected near an indoor sports complex, *Environmental*  
 447 *Science: Processes & Impacts*, 25, 304–313, <https://doi.org/10.1039/D2EM00411A>, 2023.
- 448 Anderson, L. and Fahey, D.: Studies with nitryl hypochlorite: Thermal dissociation rate and catalytic conversion to nitric oxide  
 449 using an NO/O<sub>3</sub> chemiluminescence detector, *Journal of Physical Chemistry*, 94, 644–652, 1990.
- 450 Atkinson, R., Baulch, D. L., Cox, R. A., Hampson, R. F., Jr., Kerr, J. A., and Troe, J.: Evaluated Kinetic and Photochemical  
 451 Data for Atmospheric Chemistry: Supplement IV. IUPAC Subcommittee on Gas Kinetic Data Evaluation for Atmospheric  
 452 Chemistry, *Journal of Physical and Chemical Reference Data*, 21, 1125, <https://doi.org/10.1063/1.555918>, 1992.
- 453 Atkinson, R., Baulch, D. L., Cox, R. A., Crowley, J. N., Hampson, R. F., Hynes, R. G., Jenkin, M. E., Rossi, M. J., and Troe,  
 454 J.: Evaluated kinetic and photochemical data for atmospheric chemistry: Volume I - gas phase reactions of O<sub>x</sub>, HO<sub>x</sub>, NO<sub>x</sub> and  
 455 SO<sub>x</sub> species, *Atmospheric Chemistry and Physics*, 4, 1461–1738, <https://doi.org/10.5194/acp-4-1461-2004>, 2004.
- 456 Atkinson, R., Baulch, D. L., Cox, R. A., Crowley, J. N., Hampson, R. F., Hynes, R. G., Jenkin, M. E., Rossi, M. J., Troe, J.,  
 457 and IUPAC Subcommittee: Evaluated kinetic and photochemical data for atmospheric chemistry: Volume II - gas phase  
 458 reactions of organic species, *Atmospheric Chemistry and Physics*, 6, 3625–4055, <https://doi.org/10.5194/acp-6-3625-2006>,  
 459 2006a.
- 460 Atkinson, R., Baulch, D. L., Cox, R. A., Crowley, J. N., Hampson, R. F., Hynes, R. G., Jenkin, M. E., Rossi, M. J., Troe, J.,  
 461 and IUPAC Subcommittee: Evaluated kinetic and photochemical data for atmospheric chemistry: Volume II - gas phase  
 462 reactions of organic species, *Atmospheric Chemistry and Physics*, 6, 3625–4055, <https://doi.org/10.5194/acp-6-3625-2006>,  
 463 2006b.
- 464 Atkinson, R., Baulch, D. L., Cox, R. A., Crowley, J. N., Hampson, R. F., Hynes, R. G., Jenkin, M. E., Rossi, M. J., and Troe,  
 465 J.: Evaluated kinetic and photochemical data for atmospheric chemistry: Volume III - gas phase reactions of inorganic  
 466 halogens, *Atmospheric Chemistry and Physics*, 7, 981–1191, <https://doi.org/10.5194/acp-7-981-2007>, 2007.
- 467 Bannan, T. J., Booth, A. M., Bacak, A., Muller, J. B. A., Leather, K. E., Le Breton, M., Jones, B., Young, D., Coe, H., Allan,  
 468 J., Visser, S., Slowik, J. G., Furger, M., Prévôt, A. S. H., Lee, J., Dunmore, R. E., Hopkins, J. R., Hamilton, J. F., Lewis, A.  
 469 C., Whalley, L. K., Sharp, T., Stone, D., Heard, D. E., Fleming, Z. L., Leigh, R., Shallcross, D. E., and Percival, C. J.: The  
 470 first UK measurements of nitryl chloride using a chemical ionization mass spectrometer in central London in the summer of  
 471 2012, and an investigation of the role of Cl atom oxidation, *Journal of Geophysical Research: Atmospheres*, 120, 5638–5657,  
 472 <https://doi.org/10.1002/2014JD022629>, 2015.
- 473 Baulch, D. L., Duxbury, J., Grant, S., and Montague, D. C.: Evaluated kinetic data for high temperature reactions. Volume 4.  
 474 Homogeneous gas phase reactions of halogen- and cyanide- containing species, *J. Phys. Chem. Ref. Data*, 10, 1–721, 1981.
- 475 Baulch, D. L., Cobos, C. J., Cox, R. A., Esser, C., Frank, P., Just, Th., Kerr, J. A., Pilling, M. J., Troe, J., Walker, R. W., and  
 476 Warnatz, J.: Evaluated Kinetic Data for Combustion Modelling, *Journal of Physical and Chemical Reference Data*, 21, 411,  
 477 <https://doi.org/10.1063/1.555908>, 1992.





- 478 Baulch, D. L., Cobos, C. J., Cox, R. A., Frank, P., Hayman, G., Just, Th., Kerr, J. A., Murrells, T., Pilling, M. J., Troe, J.,  
479 Walker, R. W., and Warnatz, J.: Evaluated Kinetic Data for Combustion Modeling. Supplement I, Journal of Physical and  
480 Chemical Reference Data, 23, 847–848, <https://doi.org/10.1063/1.555953>, 1994.
- 481 Bryukov, M. G., Slagle, I. R., and Knyazev, V. D.: Kinetics of Reactions of Cl Atoms with Methane and Chlorinated Methanes,  
482 J. Phys. Chem. A, 106, 10532–10542, <https://doi.org/10.1021/jp0257909>, 2002.
- 483 Burkholder, J. B., Sander, S. P., Abbatt, J., Barker, J. R., Huie, R. E., Kolb, C. E., Kurylo, M. J., Orkin, V. L., Wilmouth, D.  
484 M., and Wine, P. H.: Chemical Kinetics and Photochemical Data for Use in Atmospheric Studies, Evaluation No. 18, JPL  
485 Publication 15-10., Jet Propulsion Laboratory, Pasadena, 2015.
- 486 Cantrell, C. A.: Technical Note: Review of methods for linear least-squares fitting of data and application to atmospheric  
487 chemistry problems, Atmospheric Chemistry and Physics, 8, 5477–5487, <https://doi.org/10.5194/acp-8-5477-2008>, 2008.
- 488 Darwent, B. B.: Bond Dissociation Energies in Simple Molecules, U.S. National Bureau of Standards, 1970.
- 489 Decker, Z. C. J., Novak, G. A., Aikin, K., Veres, P. R., Neuman, J. A., Bourgeois, I., Bui, T. P., Campuzano-Jost, P., Coggon,  
490 M. M., Day, D. A., DiGangi, J. P., Diskin, G. S., Dollner, M., Franchin, A., Fredrickson, C. D., Froyd, K. D., Gkatzelis, G. I.,  
491 Guo, H., Hall, S. R., Halliday, H., Hayden, K., Holmes, C. D., Jimenez, J. L., Kupc, A., Lindaas, J., Middlebrook, A. M.,  
492 Moore, R. H., Nault, B. A., Nowak, J. B., Pagonis, D., Palm, B. B., Peischl, J., Piel, F. M., Rickly, P. S., Robinson, M. A.,  
493 Rollins, A. W., Ryerson, T. B., Schill, G. P., Sekimoto, K., Thompson, C. R., Thornhill, K. L., Thornton, J. A., Ullmann, K.,  
494 Warneke, C., Washenfelder, R. A., Weinzierl, B., Wiggins, E. B., Williamson, C. J., Winstead, E. L., Wisthaler, A., Womack,  
495 C. C., and Brown, S. S.: Airborne Observations Constrain Heterogeneous Nitrogen and Halogen Chemistry on Tropospheric  
496 and Stratospheric Biomass Burning Aerosol, Geophysical Research Letters, 51, e2023GL107273,  
497 <https://doi.org/10.1029/2023GL107273>, 2024.
- 498 Driscoll, C. T., Mason, R. P., Chan, H. M., Jacob, D. J., and Pirrone, N.: Mercury as a Global Pollutant: Sources, Pathways,  
499 and Effects, Environ. Sci. Technol., 47, 4967–4983, <https://doi.org/10.1021/es305071v>, 2013.
- 500 Frenzel, A., Scheer, V., Sikorski, R., George, Ch., Behnke, W., and Zetzsch, C.: Heterogeneous Interconversion Reactions of  
501 BrNO<sub>2</sub>, ClNO<sub>2</sub>, Br<sub>2</sub>, and Cl<sub>2</sub>, J. Phys. Chem. A, 102, 1329–1337, <https://doi.org/10.1021/jp973044b>, 1998.
- 502 Furlani, T. C., Veres, P. R., Dawe, K. E. R., Neuman, J. A., Brown, S. S., VandenBoer, T. C., and Young, C. J.: Validation of  
503 a new cavity ring-down spectrometer for measuring tropospheric gaseous hydrogen chloride, Atmospheric Measurement  
504 Techniques, 14, 5859–5871, <https://doi.org/10.5194/amt-14-5859-2021>, 2021.
- 505 Guelachvili, G., Niay, P., and Bernage, P.: Infrared bands of HCl and DCl by Fourier transform spectroscopy: Dunham  
506 coefficients for HCl, DCl, and TCl, Journal of Molecular Spectroscopy, 85, 271–281, [https://doi.org/10.1016/0022-2852\(81\)90200-9](https://doi.org/10.1016/0022-2852(81)90200-9), 1981.
- 508 Hagen, C. L., Lee, B. C., Franka, I. S., Rath, J. L., VandenBoer, T. C., Roberts, J. M., Brown, S. S., and Yalin, A. P.: Cavity  
509 ring-down spectroscopy sensor for detection of hydrogen chloride, Atmospheric Measurement Techniques, 7, 345–357,  
510 <https://doi.org/10.5194/amt-7-345-2014>, 2014.
- 511 Halfacre, J. W. and Simpson, W. R.: Polar Tropospheric Ozone Depletion Events, in: Chemistry in the Cryosphere, vol.  
512 Volume 3, WORLD SCIENTIFIC, 411–452, [https://doi.org/10.1142/9789811230134\\_0008](https://doi.org/10.1142/9789811230134_0008), 2022.
- 513 Halfacre, J. W., Stewart, J., Herndon, S. C., Roscioli, J. R., Dyroff, C., Yacovitch, T. I., Flynn, M., Andrews, S. J., Brown, S.  
514 S., Veres, P. R., and Edwards, P. M.: Using tunable infrared laser direct absorption spectroscopy for ambient hydrogen chloride  
515 detection: HCl-TILDAS, Atmospheric Measurement Techniques, 16, 1407–1429, <https://doi.org/10.5194/amt-16-1407-2023>,  
516 2023.
- 517 Heimerl, J. M. and Coffee, T. P.: The unimolecular ozone decomposition reaction, Combustion and Flame, 35, 117–123,  
518 [https://doi.org/10.1016/0010-2180\(79\)90015-4](https://doi.org/10.1016/0010-2180(79)90015-4), 1979.
- 519 Huffman, J. A., Docherty, K. S., Aiken, A. C., Cubison, M. J., Ulbrich, I. M., DeCarlo, P. F., Sueper, D., Jayne, J. T., Worsnop,  
520 D. R., Ziemann, P. J., and Jimenez, J. L.: Chemically-resolved aerosol volatility measurements from two megacity field studies,  
521 Atmos. Chem. Phys., 9, 7161–7182, <https://doi.org/10.5194/acp-9-7161-2009>, 2009.



- Ianni, J. C.: - A comparison of the Bader-Deuflhard and the Cash-Karp Runge-Kutta integrators for the GRI-MECH 3.0 model based on the chemical kinetics code Kintecus, in: Computational Fluid and Solid Mechanics 2003, edited by: Bathe, K. J., Elsevier Science Ltd, Oxford, 1368–1372, <https://doi.org/10.1016/B978-008044046-0.50335-3>, 2003.
- Ianni, J. C.: Kintecus, 2022.
- Jaeglé, L., Shah, V., Thornton, J. A., Lopez-Hilfiker, F. D., Lee, B. H., McDuffie, E. E., Fibiger, D., Brown, S. S., Veres, P., Sparks, T. L., Ebben, C. J., Wooldridge, P. J., Kenagy, H. S., Cohen, R. C., Weinheimer, A. J., Campos, T. L., Montzka, D. D., Digangi, J. P., Wolfe, G. M., Hanisco, T., Schroder, J. C., Campuzano-Jost, P., Day, D. A., Jimenez, J. L., Sullivan, A. P., Guo, H., and Weber, R. J.: Nitrogen Oxides Emissions, Chemistry, Deposition, and Export Over the Northeast United States During the WINTER Aircraft Campaign, *Journal of Geophysical Research: Atmospheres*, 123, 12,368–12,393, <https://doi.org/10.1029/2018JD029133>, 2018.
- Ji, Y., Huey, L. G., Tanner, D. J., Lee, Y. R., Veres, P. R., Neuman, J. A., Wang, Y., and Wang, X.: A vacuum ultraviolet ion source (VUV-IS) for iodide–chemical ionization mass spectrometry: a substitute for radioactive ion sources, *Atmospheric Measurement Techniques*, 13, 3683–3696, <https://doi.org/10.5194/amt-13-3683-2020>, 2020.
- Kercher, J. P., Riedel, T. P., and Thornton, J. A.: Chlorine activation by N<sub>2</sub>O<sub>5</sub>: simultaneous, in situ detection of ClNO<sub>2</sub> and N<sub>2</sub>O<sub>5</sub> by chemical ionization mass spectrometry, *Atmospheric Measurement Techniques*, 2, 193–204, <https://doi.org/10.5194/amt-2-193-2009>, 2009.
- Le Breton, M., Hallquist, Å. M., Pathak, R. K., Simpson, D., Wang, Y., Johansson, J., Zheng, J., Yang, Y., Shang, D., Wang, H., Liu, Q., Chan, C., Wang, T., Bannan, T. J., Priestley, M., Percival, C. J., Shallcross, D. E., Lu, K., Guo, S., Hu, M., and Hallquist, M.: Chlorine oxidation of VOCs at a semi-rural site in Beijing: significant chlorine liberation from ClNO<sub>2</sub> and subsequent gas- and particle-phase Cl–VOC production, *Atmospheric Chemistry and Physics*, 18, 13013–13030, <https://doi.org/10.5194/acp-18-13013-2018>, 2018.
- Lee, B. H., Lopez-Hilfiker, F. D., Mohr, C., Kurtén, T., Worsnop, D. R., and Thornton, J. A.: An Iodide-Adduct High-Resolution Time-of-Flight Chemical-Ionization Mass Spectrometer: Application to Atmospheric Inorganic and Organic Compounds, *Environ. Sci. Technol.*, 48, 6309–6317, <https://doi.org/10.1021/es500362a>, 2014.
- Lee, B. H., Lopez-Hilfiker, F. D., Schroder, J. C., Campuzano-Jost, P., Jimenez, J. L., McDuffie, E. E., Fibiger, D. L., Veres, P. R., Brown, S. S., Campos, T. L., Weinheimer, A. J., Flocke, F. F., Norris, G., O'Mara, K., Green, J. R., Fiddler, M. N., Bililign, S., Shah, V., Jaeglé, L., and Thornton, J. A.: Airborne Observations of Reactive Inorganic Chlorine and Bromine Species in the Exhaust of Coal-Fired Power Plants, *Journal of Geophysical Research: Atmospheres*, 123, 11,225–11,237, <https://doi.org/10.1029/2018JD029284>, 2018a.
- Lee, B. H., Lopez-Hilfiker, F. D., Veres, P. R., McDuffie, E. E., Fibiger, D. L., Sparks, T. L., Ebben, C. J., Green, J. R., Schroder, J. C., Campuzano-Jost, P., Iyer, S., D'Ambro, E. L., Schobesberger, S., Brown, S. S., Wooldridge, P. J., Cohen, R. C., Fiddler, M. N., Bililign, S., Jimenez, J. L., Kurtén, T., Weinheimer, A. J., Jaeglé, L., and Thornton, J. A.: Flight Deployment of a High-Resolution Time-of-Flight Chemical Ionization Mass Spectrometer: Observations of Reactive Halogen and Nitrogen Oxide Species, *Journal of Geophysical Research: Atmospheres*, 123, 7670–7686, <https://doi.org/10.1029/2017JD028082>, 2018b.
- Liao, J., Huey, L. G., Liu, Z., Tanner, D. J., Cantrell, C. A., Orlando, J. J., Flocke, F. M., Shepson, P. B., Weinheimer, A. J., Hall, S. R., Ullmann, K., Beine, H. J., Wang, Y., Ingall, E. D., Stephens, C. R., Hornbrook, R. S., Apel, E. C., Riemer, D., Fried, A., Mauldin III, R. L., Smith, J. N., Staebler, R. M., Neuman, J. A., and Nowak, J. B.: High levels of molecular chlorine in the Arctic atmosphere, *Nature Geosci.*, 7, 91–94, <https://doi.org/10.1038/ngeo2046>, 2014.
- Liu, X., Qu, H., Huey, L. G., Wang, Y., Sjostedt, S., Zeng, L., Lu, K., Wu, Y., Hu, M., Shao, M., Zhu, T., and Zhang, Y.: High Levels of Daytime Molecular Chlorine and Nitryl Chloride at a Rural Site on the North China Plain, *Environ. Sci. Technol.*, 51, 9588–9595, <https://doi.org/10.1021/acs.est.7b03039>, 2017.
- Mahmud, K., Kim, J. S., and Fontijn, A.: A high-temperature photochemical kinetics study of the oxygen atom+ hydrogen chloride reaction from 350 to 1480 K, *Journal of Physical Chemistry*, 94, 2994–2998, 1990.
- Manion, J. A., Huie, R. E., Levin, R. D., Burgess Jr., D. R., Orkin, V. L., Tsang, W., McGivern, W. S., Hudgens, J. W., Knyazev, V. D., Atkinson, D. B., Chai, E., Tereza, A. M., Lin, C.-Y., Allison, T. C., Mallard, W. G., Westley, F., Herron, J. T., Hampson, R. F., and Frizzell, D. H.: NIST Chemical Kinetics Database (NIST Standard Reference Database 17, Version 7.0 (Web Version), Release 1.6.8, Data version 2015.09), 2015.



- McManus, J. B., Zahniser, M. S., and Nelson, D. D.: Dual quantum cascade laser trace gas instrument with astigmatic Herriott cell at high pass number, *Appl. Opt.*, 50, A74, <https://doi.org/10.1364/AO.50.000A74>, 2011.
- McManus, J. B., Zahniser, M. S., Nelson, D. D., Shorter, J. H., Herndon, S. C., Jervis, D., Agnese, M., McGovern, R., Yacovitch, T. I., and Roscioli, J. R.: Recent progress in laser-based trace gas instruments: performance and noise analysis, *Appl. Phys. B*, 119, 203–218, <https://doi.org/10.1007/s00340-015-6033-0>, 2015.
- McNamara, S. M., Kolesar, K. R., Wang, S., Kirpes, R. M., May, N. W., Gunsch, M. J., Cook, R. D., Fuentes, J. D., Hornbrook, R. S., Apel, E. C., China, S., Laskin, A., and Pratt, K. A.: Observation of Road Salt Aerosol Driving Inland Wintertime Atmospheric Chlorine Chemistry, *ACS Cent. Sci.*, 6, 684–694, <https://doi.org/10.1021/acscentsci.9b00994>, 2020.
- Mielke, L. H., Furgeson, A., and Osthoff, H. D.: Observation of ClNO<sub>2</sub> in a Mid-Continental Urban Environment, *Environ. Sci. Technol.*, 45, 8889–8896, <https://doi.org/10.1021/es201955u>, 2011.
- Moravek, A., VandenBoer, T. C., Finewax, Z., Pagonis, D., Nault, B. A., Brown, W. L., Day, D. A., Handschy, A. V., Stark, H., Ziemann, P., Jimenez, J. L., de Gouw, J. A., and Young, C. J.: Reactive Chlorine Emissions from Cleaning and Reactive Nitrogen Chemistry in an Indoor Athletic Facility, *Environ. Sci. Technol.*, 56, 15408–15416, <https://doi.org/10.1021/acs.est.2c04622>, 2022.
- Osthoff, H. D., Roberts, J. M., Ravishankara, A. R., Williams, E. J., Lerner, B. M., Sommariva, R., Bates, T. S., Coffman, D., Quinn, P. K., Dibb, J. E., Stark, H., Burkholder, J. B., Talukdar, R. K., Meagher, J., Fehsenfeld, F. C., and Brown, S. S.: High levels of nitryl chloride in the polluted subtropical marine boundary layer, *Nature Geoscience*, 1, 324–328, <https://doi.org/10.1038/ngeo177>, 2008.
- Phillips, G. J., Tang, M. J., Thieser, J., Brickwedde, B., Schuster, G., Bohn, B., Lelieveld, J., and Crowley, J. N.: Significant concentrations of nitryl chloride observed in rural continental Europe associated with the influence of sea salt chloride and anthropogenic emissions, *Geophysical Research Letters*, 39, <https://doi.org/10.1029/2012GL051912>, 2012.
- R Core Team: R: A language and environment for statistical computing., 2021.
- Riedel, T. P., Bertram, T. H., Crisp, T. A., Williams, E. J., Lerner, B. M., Vlasenko, A., Li, S.-M., Gilman, J., de Gouw, J., Bon, D. M., Wagner, N. L., Brown, S. S., and Thornton, J. A.: Nitryl Chloride and Molecular Chlorine in the Coastal Marine Boundary Layer, *Environ. Sci. Technol.*, 46, 10463–10470, <https://doi.org/10.1021/es204632r>, 2012.
- Riedel, T. P., Wagner, N. L., Dubé, W. P., Middlebrook, A. M., Young, C. J., Öztürk, F., Bahreini, R., VandenBoer, T. C., Wolfe, D. E., Williams, E. J., Roberts, J. M., Brown, S. S., and Thornton, J. A.: Chlorine activation within urban or power plant plumes: Vertically resolved ClNO<sub>2</sub> and Cl<sub>2</sub> measurements from a tall tower in a polluted continental setting, *Journal of Geophysical Research: Atmospheres*, 118, 8702–8715, <https://doi.org/10.1002/jgrd.50637>, 2013.
- Riva, M., Pospisilova, V., Frege, C., Perrier, S., Bansal, P., Jorga, S., Sturm, P., Thornton, J. A., Rohner, U., and Lopez-Hilfiker, F.: Evaluation of a reduced-pressure chemical ion reactor utilizing adduct ionization for the detection of gaseous organic and inorganic species, *Atmospheric Measurement Techniques*, 17, 5887–5901, <https://doi.org/10.5194/amt-17-5887-2024>, 2024.
- Robinson, M. A., Neuman, J. A., Huey, L. G., Roberts, J. M., Brown, S. S., and Veres, P. R.: Temperature-dependent sensitivity of iodide chemical ionization mass spectrometers, *Atmospheric Measurement Techniques*, 15, 4295–4305, <https://doi.org/10.5194/amt-15-4295-2022>, 2022.
- Roscioli, J. R., Zahniser, M. S., Nelson, D. D., Herndon, S. C., and Kolb, C. E.: New Approaches to Measuring Sticky Molecules: Improvement of Instrumental Response Times Using Active Passivation, *J. Phys. Chem. A*, 120, 1347–1357, <https://doi.org/10.1021/acs.jpca.5b04395>, 2016.
- Sarwar, G., Simon, H., Bhawe, P., and Yarwood, G.: Examining the impact of heterogeneous nitryl chloride production on air quality across the United States, *Atmospheric Chemistry and Physics*, 12, 6455–6473, <https://doi.org/10.5194/acp-12-6455-2012>, 2012.
- Sarwar, G., Simon, H., Xing, J., and Mathur, R.: Importance of tropospheric ClNO<sub>2</sub> chemistry across the Northern Hemisphere, *Geophysical Research Letters*, 41, 4050–4058, <https://doi.org/10.1002/2014GL059962>, 2014.



- 614 Simon, H., Kimura, Y., McGaughey, G., Allen, D. T., Brown, S. S., Osthoff, H. D., Roberts, J. M., Byun, D., and Lee, D.:  
615 Modeling the impact of  $\text{ClNO}_2$  on ozone formation in the Houston area, *J. Geophys. Res.*, 114, D00F03,  
616 <https://doi.org/10.1029/2008JD010732>, 2009.
- 617 Simpson, W. R., Brown, S. S., Saiz-Lopez, A., Thornton, J. A., and von Glasow, R.: Tropospheric Halogen Chemistry:  
618 Sources, Cycling, and Impacts, *Chem. Rev.*, 115, 4035–4062, <https://doi.org/10.1021/cr5006638>, 2015.
- 619 Sommariva, R., Hollis, L. D. J., Sherwen, T., Baker, A. R., Ball, S. M., Bandy, B. J., Bell, T. G., Chowdhury, M. N., Cordell,  
620 R. L., Evans, M. J., Lee, J. D., Reed, C., Reeves, C. E., Roberts, J. M., Yang, M., and Monks, P. S.: Seasonal and geographical  
621 variability of nitryl chloride and its precursors in Northern Europe, *Atmospheric Science Letters*, 19, e844,  
622 <https://doi.org/10.1002/asl.844>, 2018.
- 623 Srinivasan, N. K., Su, M.-C., Sutherland, J. W., and Michael, J. V.: Reflected Shock Tube Studies of High-Temperature Rate  
624 Constants for  $\text{OH} + \text{CH}_4 \rightarrow \text{CH}_3 + \text{H}_2\text{O}$  and  $\text{CH}_3 + \text{NO}_2 \rightarrow \text{CH}_3\text{O} + \text{NO}$ , *J. Phys. Chem. A*, 109, 1857–1863,  
625 <https://doi.org/10.1021/jp040679j>, 2005.
- 626 Tan, Z., Fuchs, H., Hofzumahaus, A., Bloss, W. J., Bohn, B., Cho, C., Hohaus, T., Holland, F., Lakshmisha, C., Liu, L., Monks,  
627 P. S., Novelli, A., Niether, D., Rohrer, F., Tillmann, R., Valkenburg, T. S. E., Vardhan, V., Kiendler-Scharr, A., Wahner, A.,  
628 and Sommariva, R.: Seasonal variation in nitryl chloride and its relation to gas-phase precursors during the JULIAC campaign  
629 in Germany, *Atmospheric Chemistry and Physics*, 22, 13137–13152, <https://doi.org/10.5194/acp-22-13137-2022>, 2022.
- 630 Thaler, R. D., Mielke, L. H., and Osthoff, H. D.: Quantification of Nitryl Chloride at Part Per Trillion Mixing Ratios by  
631 Thermal Dissociation Cavity Ring-Down Spectroscopy, *Anal. Chem.*, 83, 2761–2766, <https://doi.org/10.1021/ac200055z>,  
632 2011.
- 633 Tham, Y. J., Wang, Z., Li, Q., Yun, H., Wang, W., Wang, X., Xue, L., Lu, K., Ma, N., Bohn, B., Li, X., Kecorius, S., Größ,  
634 J., Shao, M., Wiedensohler, A., Zhang, Y., and Wang, T.: Significant concentrations of nitryl chloride sustained in the morning:  
635 investigations of the causes and impacts on ozone production in a polluted region of northern China, *Atmospheric Chemistry*  
636 *and Physics*, 16, 14959–14977, <https://doi.org/10.5194/acp-16-14959-2016>, 2016.
- 637 Tham, Y. J., Wang, Z., Li, Q., Wang, W., Wang, X., Lu, K., Ma, N., Yan, C., Kecorius, S., Wiedensohler, A., Zhang, Y., and  
638 Wang, T.: Heterogeneous  $\text{N}_2\text{O}_5$  uptake coefficient and production yield of  $\text{ClNO}_2$  in polluted northern China: roles of aerosol  
639 water content and chemical composition, *Atmospheric Chemistry and Physics*, 18, 13155–13171, <https://doi.org/10.5194/acp-18-13155-2018>, 2018.
- 641 Thornton, J. A., Kercher, J. P., Riedel, T. P., Wagner, N. L., Cozic, J., Holloway, J. S., Dubé, W. P., Wolfe, G. M., Quinn, P.  
642 K., Middlebrook, A. M., Alexander, B., and Brown, S. S.: A large atomic chlorine source inferred from mid-continental  
643 reactive nitrogen chemistry, *Nature*, 464, 271–274, <https://doi.org/10.1038/nature08905>, 2010.
- 644 Troe, J.: Refined Representation of Falloff Curves for the Reaction  $\text{HO} + \text{NO}_2 + \text{N}_2 \rightarrow (\text{HONO}_2, \text{HOONO}) + \text{N}_2$ , *J. Phys.*  
645 *Chem. A*, 116, 6387–6393, <https://doi.org/10.1021/jp212095n>, 2012.
- 646 Wagner, N. L., Riedel, T. P., Young, C. J., Bahreini, R., Brock, C. A., Dubé, W. P., Kim, S., Middlebrook, A. M., Öztürk, F.,  
647 Roberts, J. M., Russo, R., Sive, B., Swarthout, R., Thornton, J. A., VandenBoer, T. C., Zhou, Y., and Brown, S. S.:  $\text{N}_2\text{O}_5$   
648 uptake coefficients and nocturnal  $\text{NO}_2$  removal rates determined from ambient wintertime measurements, *Journal of*  
649 *Geophysical Research: Atmospheres*, 118, 9331–9350, <https://doi.org/10.1002/jgrd.50653>, 2013.
- 650 Wallington, T., Ammann, M., Cox, R. A., Crowley, J. N., Herrmann, H., Jenkin, M. E., McNeill, V. F., Mellouki, A. W., and  
651 Troe, J.: Evaluated Kinetic Data for Atmospheric Chemistry, 2021.
- 652 Wang, C., Liggio, J., Wentzell, J. J. B., Jorga, S., Folkerson, A., and Abbatt, J. P. D.: Chloramines as an important  
653 photochemical source of chlorine atoms in the urban atmosphere, *Proceedings of the National Academy of Sciences*, 120,  
654 e2220889120, <https://doi.org/10.1073/pnas.2220889120>, 2023.
- 655 Wang, H., Yuan, B., Zheng, E., Zhang, X., Wang, J., Lu, K., Ye, C., Yang, L., Huang, S., Hu, W., Yang, S., Peng, Y., Qi, J.,  
656 Wang, S., He, X., Chen, Y., Li, T., Wang, W., Huangfu, Y., Li, X., Cai, M., Wang, X., and Shao, M.: Formation and impacts  
657 of nitryl chloride in Pearl River Delta, *Atmospheric Chemistry and Physics*, 22, 14837–14858, <https://doi.org/10.5194/acp-22-14837-2022>, 2022.



- 659 Wang, T., Tham, Y. J., Xue, L., Li, Q., Zha, Q., Wang, Z., Poon, S. C. N., Dubé, W. P., Blake, D. R., Louie, P. K. K., Luk, C.  
660 W. Y., Tsui, W., and Brown, S. S.: Observations of nitryl chloride and modeling its source and effect on ozone in the planetary  
661 boundary layer of southern China:  $\text{ClNO}_2$  IN PBL OF CHINA, *J. Geophys. Res. Atmos.*, 121, 2476–2489,  
662 <https://doi.org/10.1002/2015JD024556>, 2016.
- 663 Wang, X., Jacob, D. J., Eastham, S. D., Sulprizio, M. P., Zhu, L., Chen, Q., Alexander, B., Sherwen, T., Evans, M. J., Lee, B.  
664 H., Haskins, J. D., Lopez-Hilfiker, F. D., Thornton, J. A., Huey, G. L., and Liao, H.: The role of chlorine in global tropospheric  
665 chemistry, *Atmospheric Chemistry and Physics*, 19, 3981–4003, <https://doi.org/10.5194/acp-19-3981-2019>, 2019.
- 666 Wang, X., Jacob, D. J., Downs, W., Zhai, S., Zhu, L., Shah, V., Holmes, C. D., Sherwen, T., Alexander, B., Evans, M. J.,  
667 Eastham, S. D., Neuman, J. A., Veres, P. R., Koenig, T. K., Volkamer, R., Huey, L. G., Bannan, T. J., Percival, C. J., Lee, B.  
668 H., and Thornton, J. A.: Global tropospheric halogen (Cl, Br, I) chemistry and its impact on oxidants, *Atmospheric Chemistry*  
669 *and Physics*, 21, 13973–13996, <https://doi.org/10.5194/acp-21-13973-2021>, 2021.
- 670 Wang, Z., Wang, W., Tham, Y. J., Li, Q., Wang, H., Wen, L., Wang, X., and Wang, T.: Fast heterogeneous  $\text{N}_2\text{O}_5$  uptake and  
671  $\text{ClNO}_2$  production in power plant and industrial plumes observed in the nocturnal residual layer over the North China Plain,  
672 *Atmospheric Chemistry and Physics*, 17, 12361–12378, <https://doi.org/10.5194/acp-17-12361-2017>, 2017.
- 673 Wilkerson, J., Sayres, D. S., Smith, J. B., Allen, N., Rivero, M., Greenberg, M., Martin, T., and Anderson, J. G.: In situ  
674 observations of stratospheric HCl using three-mirror integrated cavity output spectroscopy, *Atmospheric Measurement*  
675 *Techniques Discussions*, 1–38, <https://doi.org/10.5194/amt-2021-6>, 2021.
- 676 Xia, M., Peng, X., Wang, W., Yu, C., Sun, P., Li, Y., Liu, Y., Xu, Z., Wang, Z., Xu, Z., Nie, W., Ding, A., and Wang, T.:  
677 Significant production of  $\text{ClNO}_2$  and possible source of  $\text{Cl}_2$  from  $\text{N}_2\text{O}_5$  uptake at a suburban site in eastern China, *Atmospheric*  
678 *Chemistry and Physics*, 20, 6147–6158, <https://doi.org/10.5194/acp-20-6147-2020>, 2020.
- 679 Xiao, F., Sasi, P. C., Yao, B., Kubátová, A., Golovko, S. A., Golovko, M. Y., and Soli, D.: Thermal Stability and  
680 Decomposition of Perfluoroalkyl Substances on Spent Granular Activated Carbon, *Environ. Sci. Technol. Lett.*, 7, 343–350,  
681 <https://doi.org/10.1021/acs.estlett.0c00114>, 2020.
- 682 Ye, C., Yuan, B., Lin, Y., Wang, Z., Hu, W., Li, T., Chen, W., Wu, C., Wang, C., Huang, S., Qi, J., Wang, B., Wang, C., Song,  
683 W., Wang, X., Zheng, E., Krechmer, J. E., Ye, P., Zhang, Z., Wang, X., Worsnop, D. R., and Shao, M.: Chemical  
684 characterization of oxygenated organic compounds in the gas phase and particle phase using iodide CIMS with FIGAERO in  
685 urban air, *Atmospheric Chemistry and Physics*, 21, 8455–8478, <https://doi.org/10.5194/acp-21-8455-2021>, 2021.
- 686 Young, C. J., Washenfelder, R. A., Roberts, J. M., Mielke, L. H., Osthoff, H. D., Tsai, C., Pikelnaya, O., Stutz, J., Veres, P.  
687 R., Cochran, A. K., VandenBoer, T. C., Flynn, J., Grossberg, N., Haman, C. L., Lefer, B., Stark, H., Graus, M., de Gouw, J.,  
688 Gilman, J. B., Kuster, W. C., and Brown, S. S.: Vertically Resolved Measurements of Nighttime Radical Reservoirs in Los  
689 Angeles and Their Contribution to the Urban Radical Budget, *Environ. Sci. Technol.*, 46, 10965–10973,  
690 <https://doi.org/10.1021/es302206a>, 2012.
- 691 Yu, C., Wang, Z., Xia, M., Fu, X., Wang, W., Tham, Y. J., Chen, T., Zheng, P., Li, H., Shan, Y., Wang, X., Xue, L., Zhou, Y.,  
692 Yue, D., Ou, Y., Gao, J., Lu, K., Brown, S. S., Zhang, Y., and Wang, T.: Heterogeneous  $\text{N}_2\text{O}_5$  reactions on atmospheric  
693 aerosols at four Chinese sites: improving model representation of uptake parameters, *Atmospheric Chemistry and Physics*, 20,  
694 4367–4378, <https://doi.org/10.5194/acp-20-4367-2020>, 2020.
- 695 Zhou, W., Zhao, J., Ouyang, B., Mehra, A., Xu, W., Wang, Y., Bannan, T. J., Worrall, S. D., Priestley, M., Bacak, A., Chen,  
696 Q., Xie, C., Wang, Q., Wang, J., Du, W., Zhang, Y., Ge, X., Ye, P., Lee, J. D., Fu, P., Wang, Z., Worsnop, D., Jones, R.,  
697 Percival, C. J., Coe, H., and Sun, Y.: Production of  $\text{N}_2\text{O}_5$  and  $\text{ClNO}_2$  in summer in urban Beijing, China, *Atmospheric*  
698 *Chemistry and Physics*, 18, 11581–11597, <https://doi.org/10.5194/acp-18-11581-2018>, 2018.